RU-79-134 E-154
FERMILAB-PUB-80-112-E

Neutral Particle Production in $\pi^- p$ Interactions at 147 GeV/c and Comparison to Charged Particle Production

D. Brick, D. Fong,* M. Heller,† A. M. Shapiro, and M. Widgoff
Brown University, Providence, Rhode Island 02912

F. Bruyant
CERN, Geneva 23, Switzerland

D. Bogert and M. Johnson
Fermilab, Batavia, Illinois 60510

R. Burnstein, C. Fu,‡ D. Petersen,§ M. Robertson,‖ and H. Rubin
Illinois Institute of Technology, Chicago, Illinois 60616

R. Sard, A. Snyder,¶ and J. Tortora**
University of Illinois, Urbana, Illinois 61801

E. D. Alyea, Jr.
Indiana University, Bloomington, Indiana 47401

C.-Y. Chien, P. Lucas,†† A. Pevsner, and R. Żdanis
Johns Hopkins University, Baltimore, Maryland 21218

F. Barreiro,* O. Benary,‖‖ J. E. Brau,§§ J. Grunhaus,‖‖ E. S. Hafen, R. I. Hulsizer, U. Karshon,¶¶ V. Kistiakowsky, A. Levy,‡‡ A. Napier, I. A. Pless, J. P. Silverman,§§§ P. C. Trepagnier, J. Wolfson,*** and R. K. Yamamoto
Massachusetts Institute of Technology, Cambridge, Massachusetts 02139

H. Cohn
Oak Ridge National Laboratory, Oak Ridge, Tennessee 37830

P. F. Jacques, T. C. Ou, R. J. Plano, and T. L. Watts
Rutgers University, New Brunswick, New Jersey 08903

E. B. Brucker, E. L. Koller, P. Stamer, and S. Taylor
Stevens Institute of Technology, Hoboken, New Jersey 07030

RECEIVED
JUL 11 1979
DIRECTORS OFFICE
FERMILAB

W. Bugg, G. Condo, T. Handler, and E. Hart
University of Tennessee, Knoxville, Tennessee 37916

H. Kraybill, D. Ljung, T. Ludlum[†††], and H. D. Taft
Yale University, New Haven, Connecticut 06520

[*]Present address: DESY, Hamburg, West Germany.
[†]Present address: New England Nuclear, Billerica, Massachusetts.
[‡]Present address: Polytechnic Institute of New York, Brooklyn New York.
[§]Present address: Indiana University, Bloomington, Indiana.
[‖]Present address: Purdue University, West Lafayette, Indiana.
[¶]Present address: Argonne National Laboratory, Argonne, Illinois.
[**]Present address: Dialog Systems, Inc., Belmont, Massachusetts.
[††]Present address: Duke University, Durham, North Carolina.
[‡‡]On leave of absence from Tel-Aviv University, Israel.
[§§]Present address: Stanford Linear Accelerator Center, Stanford, California.
[‖‖]Present address: Tel-Aviv University, Israel.
[¶¶]Present address: Weizmann Institute of Science, Rehovot, Israel.
[***]Present address: Fermilab, Batavia, Illinois.
[§§§]Present address: Rockefeller University, N.Y., N.Y.
[†††]Present address: CERN, Geneva, Switzerland.

ABSTRACT

The production of K_s, Λ, $\bar{\Lambda}$ and γ in $\pi^- p$ collisions at 147 GeV/c is analyzed. Cross-sections, rapidity, Feynman x and p_T^2 distributions are presented and compared to charged particle production. The energy dependence of multiplicities in $\pi^- p$ and pp collisions is shown. A new scaling form for the correlation of neutral and charged particle multiplicities is presented for compilations of πp and pp data.

I. Introduction and Summary

We present final results on inclusive neutral particle production in $\pi^- p$ collisions at 147 GeV/c in the 30 in Hybrid Spectrometer at Fermilab[1], and make comparisons in energy, between πp and pp collisions, between neutral and charged particle distributions, and among the neutral particle results. Past studies[2] on K_s, Λ, $\bar{\Lambda}$ and γ inclusive production have established many characteristics, and here we add results at 147 GeV/c, update some comparisons and introduce new analysis.

Inclusive cross-sections in the form of average multiplicities rise with energy except for Λ production, and pp and πp multiplicities agree, again except for Λ production. The average multiplicity of Λ's per event appears to be independent of energy and less than a ratio of 2 for pp vs πp collisions as might be expected from the ratio of incoming baryons. The average K_s multiplicity agrees with the average charged particle multiplicity as a function of energy within a constant factor. $K^{\pm}$ production does not agree.

Inclusive distributions in y, x and p_t^2 are shown and compared to charged particle production. If a rapidity plateau is assumed for K_s production, then its height agrees with the logarithmic rise in K_s multiplicity with energy.

A new scaling function derived from KNO arguments (see later) is used to analyze the energy dependence of the semi-inclusive average multiplicity of neutral particles. The new scaling function facilitates the analysis of the data in terms of K/π ratios etc. The ratio of neutral to charged particle multiplicity appears to have the same form for K_s and π° production and to be the same for

pp and πp collisions. The scaling function for the Λ multiplicity is only slightly different. The ratio of neutral to charged particle multiplicity is not constant as charged multiplicity increases but does not fall for charged multiplicities above the average as expected in some models.

Section II, following, discusses experimental details, Section III inclusive cross-sections and distributions, Section IV two-particle multiplicities.

II. Data Analysis

105K pictures were taken in this experiment, of which 79K were available for the study of events containing neutral decays and conversions. A first scan of the film was done for all events as defined in reference 3; it yielded approximately 15000 events. A second pass was performed on events containing neutral decays and conversions to check and correct the record of the event topology and to label the neutrals according to vertex type, i.e. "VO" (non-zero opening angle of decay), "straight gamma" (zero opening angle of decay in all three views), "curly gamma" (one track of pair seen to turn through 180° and to have minimum ionization throughout). The second pass was also perfomed on some 15% of total events which were rejected for the purposes of reference 3 but could not be rejected in this study of neutrals because of bias.

A completely independent scan was performed on 27K pictures, containing 28% of the beam flux, in order to determine the contribution of the scan losses to the cross-sections, distributions, etc. The events lost from the first scan were measured carefully and their contributions to cross-sections etc. increased by the factor 1/0.28. The first scan's efficiency for neutral vertices computed in the usual fashion, was 78%; the scan efficiency for the combined data in the 27K pictures was (98.9 ± 0.4)%. Table I shows the sources of neutral vertices from these passes and scans.

Events found during the scan phases described above were then measured on the Rutgers PEPR[4]. Tracks from neutral decays and conversions for all events, and charged secondary tracks from 2, 4, 6

prong events were always measured. Charged secondary tracks from events with 8 or more prongs were measured only for events containing strange particles (K_s^o, Λ, $\bar{\Lambda}$) and only in the 27K sample of pictures. Data from the charged tracks are not used in the analysis in this paper.

Reconstruction of tracks in the bubble chamber and wire chambers was done by the program chain GEOMAT-PWGP-TKORG[3]. No attempt was made in this reconstruction to find parts of neutral decay tracks which entered the wire chambers - only tracks from the primary vertex were reconstructed in both bubble and wire chambers. Program SQUAW was used to identify the neutral particle using the usual 3C and 1C fits:

$$K_s^o \rightarrow \pi^+\pi^- \tag{1a}$$

$$\Lambda \rightarrow p\pi^- \tag{1b}$$

$$\bar{\Lambda} \rightarrow \bar{p}\pi^+ \tag{1c}$$

$$\gamma p \rightarrow e^+e^-p \tag{1d}$$

In order to obtain satisfactory distributions of residual errors after the fit ("pull" distributions) it was necessary to increase the input error matrices on all momenta and vertex coordinates by a factor of 2 and to add constant amounts to the errors on y and z coordinates of vertices of $\Delta y = 170$ μm and $\Delta z = 850$ μm (the z-direction is along the camera axis and the y direction is perpendicular to beam and z).

A decay volume cut on the decay vertex was applied at x = 25 cm in order to provide approximately 15 cm of visible length of decay track for reconstruction and fitting, and a minimum length cut of 2

cm was applied to neutral tracks to avoid losses of neutral vertices too close to the primary vertex. All fits were inspected at the scan table for consistency with ionization and with topological type (zero opening angle, identified electron, etc) and for poorly measured data. Events which failed this inspection or failed to give a fit were remeasured carefully in the sample of 27K pictures mentioned previously and their contributions to distributions again scaled up. In this sample of 27K pictures, 20% of all events were remeasured because of such a measuring failure; failures occurred more often among those events with fast neutrals in the forward jet of charged particles. Fig. 1 shows the c.m. rapidity distribution of the re-scan and remeasured events (shaded) compared to the overall distributions; some bias towards the forward direction can be seen. About 2% of events in the 27K sample failed remeasurement and were not tried again.

The chi-squared probability distributions for the 3c fits which passed the decay volume cut are shown in Fig. 2; the excess of events at low probability is presumably another manifestation of the error assignment problem. Some 13% of the final accepted sample of neutrals failed to give 3c fits but gave 1c fits and were believed to point back to the primary vertex by the physicist who looked at the event on the scan table. This failure seems related to the incorrect assignment of errors on the vertices. We have included these 1c events in the cross-sections and distributions since we believe their momenta are accurate enough for the studies included here.

Neutral vertices which fitted more than one decay process consistent with ionization and topology type ("ambiguous fits") were

assigned by the following ordered tests:

(i) a gamma fit, if present, was selected if the transverse momentum of the negative track with respect to the direction of the neutral was less than 25 MeV/c. Gamma fits were rejected for the transverse momenta above 25 MeV/c.

(ii) a K_S^O fit was selected if the negative track transverse momentum was greater than 105 MeV/c.

(iii) the $\bar{\Lambda}$ fit was only selected if its χ^2 probability was at least three times that of the competing fits. This criterion was chosen to keep the ratio of ambiguous $\bar{\Lambda}$ fits to ambiguous K_S^O and Λ fits the same as the overall numbers of $\bar{\Lambda}$, K_S^O and Λ fits in order to avoid too large a ratio of ambiguous to unambiguous $\bar{\Lambda}$ fits. One event was assigned to a $\bar{\Lambda}$ decay by this criterion.

(iv) K_S^O/Λ ambiguities were resolved by satisfying two conditions - the ratio of K_S^O decays with transverse π^- momentum below 105 MeV/c to those above 105 MeV/c should be given by the theoretical value of 14% for a spinless decay; secondly, we should expect K_S^O decays to simulate a $\bar{\Lambda}$ decay as often as a Λ decay. Both conditions could not be satisfied simultaneously, so we have resolved the K/Λ ambiguities so that neither condition is badly violated. The criterion for a K_S^O decay, then, is that the K_S^O fitted probability is greater than 1.43 times that of the Λ fit; this choice resolves 56 ambiguous neutrals into 46 Λ fits and 10 K_S^O fits.

Cross-sections and distributions have been calculated in the usual fashion by assigning weights to neutrals to correct for their detection efficiency. The average detection weights were K_S^O: 2.03, Λ: 2.12, $\bar{\Lambda}$: 2.77, γ: 55.4. Other weighting factors accounted for the branching ratios of decays and for the method of partial remeasurement described earlier. Conversion to cross-sections, viz μb/event, were taken from reference 3 (1.43 μb/event for 2 prongs, 1.59 μb/event for other prongs).

As a check on quality of data, the decay angle distributions for K_S^O, Λ, and $\bar{\Lambda}$ and the negative track transverse momentum distributions of all 4 neutral types are shown in Figs. 3 and 4. The decay angles, Fig. 3, are obtained in the particles' rest frame with z along the direction of the neutral, and x perpendicular to the camera axis, and are calculated for the negative decay particle. They are acceptably flat in both angles for K_S^O and Λ and in azimuth angle for $\bar{\Lambda}$ as expected - there is little sign of the usual loss at azimuthal angle = $\pm\pi/2$. Fig. 4 shows the momentum component of the negative track transverse to the line of flight of the neutral; again the experimental distributions agree with expected distributions.

III. Cross-sections and Inclusive Distributions

Inclusive cross-sections are shown in Table II. The Λ cross-section includes Λ production from Σ^0 decays. Errors shown are mainly statistical but include contributions from estimates of contamination and of the reliability of weighting schemes: contamination has been checked by looking for K_s^0, Λ, $\bar{\Lambda}$ and γ invariant mass enhancements in each of the alternative categories - the worst cases were for $\bar{\Lambda}$ where 10% of the events could be γ contamination, and γ where 1/2% of the K_s^0 events could have been mis-classified as γ's. These contaminations are small compared to the statistical error. The weighting schemes, including effects of decay volume, are estimated to contribute 5% uncertainties in the cross-sections. Two particle inclusive cross-sections are also given in Table II.

Comparison of the cross-sections with those for pp collisions and for πp collisions at other energies is shown in the form of average multiplicity in Fig. 5 for Λ, $\bar{\Lambda}$ and γ production, and in Fig. 6 for K_s production. The fit to π^0 multiplicity $\langle\pi^0\rangle$ is from Whitmore[5] and, in Fig. 6, the fits to K_s multiplicity will be discussed below. The sources of the data are tabulated in reference 6. The cross-sections from this experiment agree within the errors with the general trends shown in Figs. 5 and 6.

The general trends of the cross-sections are for rising average multiplicity as energy increases for all particles, except for Λ's above laboratory momentum of 50 GeV/c. In addition πp and pp collisions agree, except for Λ production which is presumably influenced by the difference in baryon number in the initial πp and pp states.

If we average the multiplicity of Λ's above laboratory momenta of 40 GeV/c then the ratio is $(pp \to \langle\Lambda\rangle)/(\pi p \to \langle\Lambda\rangle) = 1.44 \pm 0.03$. If all Λ production was in the fragmentation region of protons then, naively this ratio should be 2.0. From the value of the ratio quoted above, we conclude that about half of Λ production occurs from proton fragmentation, the rest from pion fragmentation and/or central region production.

The production of K_s particles may be analyzed by comparison to pion production which constitutes most of the charged particle production. Fig. 6 shows the average K_s multiplicity $\langle n_k \rangle$ as a function of laboratory momentum for $\pi^- p$, pp and some $\pi^+ p$ collisions. A fit to the data of the form $\langle n_k \rangle = A + B \ln s$ gives the result

$$\langle n_k \rangle = (-0.086 \pm 0.011) + (0.045 \pm 0.003) \ln s$$

The fit is shown in Fig. 6 and can be seen to represent the general tendency of the data in spite of a low confidence level (χ^2 of 47.5 for 13 degrees of freedom). Comparison to charged particle production can be made by obtaining similar fits to charged particle multiplicity $\langle n_c \rangle$ and scaling this multiplicity down by a ratio of K_s to charged particle production; in this case the ratio was taken to be ratio of average multiplicities for this experiment $\langle n_k \rangle / \langle n_c \rangle = 0.175/7.40$. Fig. 6 shows scaled down fits to $\langle n_c \rangle$ in $\pi^- p$ and pp interactions[7,8]. Note that these fits to both $\pi^- p$ and pp charged multiplicities allow non-linear terms. It can be seen

FERMILAB-PUB-80-112-E

that K_s production is similar in $\pi^- p$ and pp collisions and that it is similar to the scaled down charged particle production except possibly at the highest energy in $\pi^- p$ collisions. The fits are dominated by their lns terms and this appears to be the main energy dependence for both charged and K_s multiplicities. Also shown in the graph for comparison purposes is a fit to $K^{\pm}$ multiplicities in pp collisions[8]; it can be seen that charged and neutral K multiplicities appear to have qualitatively different energy dependences.

The inclusive distributions of K_s^o, Λ, $\bar{\Lambda}$ and γ are shown as a function of c.m. rapidity y in Fig. 7, as a distribution in Feynman x in Fig. 8, and as the invariant cross-section $2E/(\sqrt{s}\pi)\ d\sigma/dx$ in Fig. 9. From the distributions it can be seen that K_s^o, $\bar{\Lambda}$ and γ are produced predominantly in the central region of rapidity whereas Λ's are produced predominantly in the fragmentation region of the proton target. The energy dependence and approach to scaling of the cross-section $(1/\pi)(d\sigma/dy)$ at $y = 0$ have been discussed by Boggild and Ferbel[9] and Whitmore[10] who assume a $s^{-1/4}$ asymptotic dependence for these cross-sections normalized by σ_{total} or $\sigma_{pomeron}$[10]. Our values for $d\sigma/dy$ and the normalized cross-section are recorded in Table III for K_s^o and for charged particle production - they agree within errors with the expected behavior and other nearby data in Ferbel's and Whitmore's normalized plots.

For Fermilab energies it is difficult to establish the existence of a rapidity plateau even for pion production. For K_s production, we indirectly investigate the plateau by comparing the lns rise in K_s multiplicity with the lns expansion of the available

rapidity and the height of the $d\sigma/dy$ distribution at $y = 0$. Table IV shows the results tabulated as density of particle production per unit of rapidity vs. multiplicity increase per unit of lns. Figure 7 also shows the height of the central plateau expected from the multiplicity increase per unit of lns. As can be seen from Table IV and Figure 7, there is rough parity between production in the central region and increases in multiplicity. Any differences are in the same direction as for charged particle production. We conclude therefore that K_s production is consistent with the existence of a rapidity plateau.

The transverse momentum squared distributions $d\sigma/dp_t^2$ for the neutrals, shown in Fig. 10, and with an expanded scale in Fig. 11, are sharply cut off just as the charged particles are. At small p_t^2, the distribution falls faster than the strange-particles which are not noticeably different from each other. At large p_t^2, all the distributions level off and are decreasing at about the same rate from 0.5 to 2.5 GeV^2

The profiles of $\langle p_t^2 \rangle$ vs. the longitudinal variables, x and y are shown in Figs. 12 and 13. The distributions for γ and K_s^o are very similar to that of the π^+ distribution shown in Figs. 14 and 15 which show a dip at $x = 0$ and constant $\langle p_t^2 \rangle$ vs. y except for y near y_{min} and y_{max}. These features are not apparent in the Λ and $\bar{\Lambda}$ distributions probably because of the limited statistics.

IV. Multiplicities of Neutral and Charged Particles

We discuss here only the correlation of neutral particle multiplicity and associated charged particle multiplicity. The dependence of charged particle multiplicity on the mass of the recoil against the neutral particle is discussed elsewhere.[11]

It has been known for some time that the average number of neutral pions is correlated with the accompanying charged multiplicity from hadron collisions at Fermilab energies.[2] The same result is also known to apply to the production of K_s particles.[2] Fig. 16 shows the average multiplicity[12] of π^o, K_s, Λ and $\bar{\Lambda}$ as a function of accompanying charged multiplicity for this experiment. Also shown for comparison are 100 GeV/c and 250 GeV/c data for $\pi^- p$ collisions. The usual strong correlation in K_s and π^o data can be seen but the correlation in the Λ data is uncertain as might be expected for baryon production.

The energy dependence of the associated neutral and charged multiplicities shown in Fig. 16 has been discussed in the form of a scaling function derived by Dao and Whitmore[13] from KNO arguments and applied to π^o production by them, and to K_s production by Cohen[14], both applications using only pp collision data. This scaling function uses the semi-inclusive cross-section for the neutral particle production and was quite well satisfied. We use an alternative scaling function based on the average multiplicity of neutral particles as a function of charged multiplicity (Fig. 16) since such a function is

closely related to the more easily interpreted $K_s/\pi^{\pm}$ or $\pi^o/\pi^{\pm}$ ratio. We first present the new function then apply it to a compilation of both pp and πp data on the production of K_s, Λ, $\bar{\Lambda}$ and π^o particles.

The KNO invariant distribution ψ for two types of particle (here taken to be charged and K_s to fix notation) is[15]

$$P_{nk} = \frac{1}{\langle n\rangle\langle k\rangle}\,\psi(z_n, z_k)$$

where $P_{nk} = \sigma_{nk}/\sigma_{inelastic}$, σ_{nk} = cross-section for events with n charged particles and k neutral K_s particles, $z_n = n/\langle n\rangle$ and $z_k = k/\langle k\rangle$. The semi-inclusive K_s cross-section is $\sum_k kP_{nk}\sigma_{inelastic}$ and the topological cross-section is $\sum_k P_{nk}\sigma_{inelastic}$ so that the average multiplicity of K_s particles in n-prong events $\langle k\rangle_n$ is

$$\langle k\rangle_n = \langle k\rangle \frac{\sum_{z_k} z_k\,\psi(z_n, z_k)}{\sum_{z_k} \psi(z_n, z_k)}$$

$$= \langle k\rangle\,\phi_3(z_n)$$

where $\phi_3(z_n)$ is a scaling function, independent of s except as $\langle n\rangle$ depends on s in $z_n = n/\langle n\rangle$. The relation of this new invariant function ϕ_3 to that previously derived by Dao and Whitmore ϕ_2, and to the charged particle invariant function of Koba, Nielsen and Olesen[15] ϕ_1 is

$$\phi_3 = \phi_2/\phi_1$$

A scaling plot can thus be made using $\langle k\rangle_n/\langle k\rangle$ vs. $n/\langle n\rangle$.

FERMILAB-PUB-80-112-E

Before inspecting data, a remark can be made about the energy dependence of the plot of n-prong average multiplicity of K_s particles $\langle k\rangle_n$ vs. n. The energy dependence of the overall average K_s multiplicity $\langle k\rangle$ as we have seen above is approximately represented by

$$\langle k\rangle = a\langle n\rangle$$

where a is a constant, and $\langle n\rangle$ increases approximately as lns. Thus given a dependence of $\langle k\rangle_n$ on n at some energy, we expect the trend with increasing energy of the plot $\langle k\rangle_n$ vs. n to be that shown in Figure 17. Such a behavior has been noted before by Whitmore for π^o production in pp collisions.[16]

Figures 18, 19, 20 and 21 show a compilation of πp and pp data[6] on K_s, π^o, Λ and $\bar{\Lambda}$ production in the scaling plot of $\langle n_o\rangle_n/\langle n_o\rangle$ vs. $n/\langle n\rangle$ where n_o is the multiplicity of neutral particles. The data are restricted to be above laboratory momentum of about 70 GeV/c but some lower energy data are discussed below. Scaling is satisfied in the energy range allowed in the plot and $\pi^- p$ and pp data agree. It is worth noting that the range over which scaling can be checked is not extensive because of the lns dependence of the scaling factors $\langle n\rangle$ and $\langle n_o\rangle$; thus the range in $\langle n\rangle$ is 6.3 to 9.3, and the change in scaling factor is about 50%.

The scaling forms for K_s and π^o data are similar and the same hand-drawn curve is added to both graphs to help in the comparison. Production of neutral and charged particles has been analysed in several models, some of which[17] predict a reduction in neutral particle production as the charged multiplicity increases above $n/\langle n\rangle = 1.0$. This clearly does not happen in the π^o data. In the K_s data however,

there are some indications of a reduction[18] in K_s multiplicity around $n/\langle n\rangle = 1.5$ to 2.0, but not in the form suggested by the models and not in all experiments. The data is inconclusive but it is important to establish if there is a difference between K_s and π^o production. A constant ratio K_s to charged particle or π^o to charged particle multiplicity would appear as a straight line on the scaling curves. Neither K_s nor π^o data show such a constant ratio.

Neutral baryon production, i.e., Λ and $\bar{\Lambda}$ multiplicity, shown in Figures 20 and 21, might be expected to differ from meson, K_s and π^o, production. Again, the same hand-drawn curve has been transferred from the K_s and π^o multiplicity graphs to these Λ and $\bar{\Lambda}$ plots. Multiplicity of Λ's is less correlated with charged particle multiplicity than for meson production. $\bar{\Lambda}$ production, however, appears to fall at multiplicities above the average.

For comparison to $K_s/\pi^{\pm}$ or $\pi^o/\pi^{\pm}$ ratios we present in Figures 22 and 23 the closely connected K_s and π^o ratios to all charged particles still normalized by $\langle n_o\rangle$ and $\langle n\rangle$ in order to keep the scaling properties previously derived. Both ratios fall with increasing charged multiplicity. The variables plotted are $(\langle n_o\rangle_n/\langle n_o\rangle)/(n/\langle n\rangle)$ vs. $n/\langle n\rangle$.

Fig. 24 presents some K_s data at low energies in the scaling plot for comparison to the high energy data in Fig. 18. The same hand-drawn curve is again transferred to this lower energy data in order to facilitate the comparison and it can be seen that the low energy data do not have the same shape as that of high energy.

Acknowledgements

This work was supported in part by the U. S. Department of Energy and the National Science Foundation. We wish to thank the personnel of the Fermilab neutrino section and the 30-inch bubble-chamber facility whose skills and efforts made this experiment possible. We also thank the personnel of the participating universities and our data reduction personnel whose dedicated skills were vital to the success of this work.

References

1. Fermilab experiment E154.
2. For compilations of data see J. Whitmore, Phys. Reports 10C (1974) 273 and Phys. Reports 27C (1976) 187.
3. D. Fong et al., Nuclear Physics B102, 386 (1976).
4. P. F. Jacques et al., Rev. Sci. Instrum. 48, 963 (1977).
5. J. Whitmore, Phys. Reports 27C (1976) 187, Figs. 38, 39.
6. Cross-sections are from publications listed below. Inelastic cross-sections are from the compilation in Rev. Mod. Phys. 47 (1975) 535.

   T. Ferbel and H. Taft, Inelastic Interactions of 11.4 GeV/c π^- Mesons in Hydrogen, Nuovo Cimento 28, 1214 (1963). F. Barreiro et al., Inclusive Neutral-Strange-Particle Production in π^-p Interactions at 15 GeV/c, Phys. Rev. D17, 669 (1978).

   P. Bosetti et al., Inclusive Strange Particle Production in π^+p Interactions at 16 GeV/c, Nuc. Phys. B94, 21 (1975).

   J. Bartke et al., Hyperon and Kaon Production by 16 GeV/c Negative Pions on Protons, Nuovo Cimento 24, 876 (1962).

   P. H. Stuntebeck et al., Inclusive Production of K_1^o, Λ^o, and $\bar{\Lambda}^o$ in 18.5 -GeV/c $\pi^{\pm}p$ Interactions, Phys. Rev. D9, 608 (1974).

   J. T. Powers et al., Compilation of Data for $\pi^{\pm}p$ Inclusive Reactions at 8 and 18.5 GeV/c, Phys. Rev. D8, 1947 (1973).

   O. Balea et al., Neutral Strange Particle Production in π^-p, π^-n, and π^-C Interactions at 40 GeV/c, Nucl. Phys. B79, 57 (1974).

   H. Blumenfeld et al., Inclusive Neutral Kaon and Lambda Production in 69 GeV/c pp Interactions, Phys. Lett. 45B 528 (1973).

H. Blumenfeld et al., Photon Production in 69 Gev/c pp Interactions, Phys. Lett. 45B 525 (1973).

V.V. Ammosov et al., Average Charged Particle Multiplicity and Topological Cross Sections in 50 Gev/c and 69 Gev/c pp Interactions, Phys. Lett. 42B 519 (1972).

E.L. Berger et al., Production of K_s^o, Λ , and γ in 100 Gev/c $\pi^- p$ Interactions, CERN/D.Ph.II/Phys 74-27 (1974).

E.L. Berger et al., Multiplicity Cross Sections for 100 Gev/c $\pi^- p$ Interactions, CERN/D.Ph.II/Phys 74-9 (1974).

J.W. Chapman et al., Production of γ , Λ^o , K_s^o, and $\bar{\Lambda}^o$ in pp Collisions at 102 Gev/c, Phys. Lett. 47B 465 (1973).

C. Bromberg et al., Cross Sections and Charged-Particle Multiplicities at 102 and 405 Gev/c, Phys. Rev. Lett. 31 1563 (1973).

D. Ljung et al., $\pi^- p$ Interactions at 205 Gev/c: Multiplicities of Charged and Neutral Particles; Production of Neutral Particles, Phys. Rev. D15 3163 (1977).

K. Jaeger et al., Characteristics of V^o and γ Productions in pp Interactions at 205 Gev/c, Phys. Rev. D11 2405 (1975).

D. Bogert et al., Inclusive Production of Neutral Strange Particles in 250 Gev/c $\pi^- p$ Interactions, Phys. Rev. D16 2098 (1977).

S. Hagopian et al., FSU - HEP - 76 - 1 - 2 (1976). Topological Cross-sections and Multiplicity Moments for $\pi^- p$ Interactions at 250 Gev/c.

A. Sheng et al., pp Interactions at 300 GeV/c: γ and Neutral-Strange-Particle Production, Phys. Rev. D11, 1733 (1975).

A. Firestone et al., pp Interactions at 300 GeV/c: Measurement of the Charged-Particle Multiplicity and the Total and Elastic Cross Sections, Phys. Rev. D10, 2080 (1974).

V. P. Kenney et al., Inclusive Production of π^o, K_s^o, Λ^o, and $\bar{\Lambda}^o$ in 360 GeV/c $\pi^- p$ Interactions. Tokyo 1978 conference. A. Firestone et al., $\pi^- p$ Interactions at 360 GeV/c: Measurement of the Total and Elastic Cross Sections and the Charged-Particle Multiplicity Distribution, Phys. Rev. D14, 2909 (1976).

7. P. Stix and T. Ferbel, Phys. Rev. D15, 358 (1977).

8. M. Antinucci et al., Lett. Nuovo Cimento 6, 121 (1973).

9. H. Boggild and T. Ferbel, Ann. Rev. Nucl. Sci. 24, 451 (1974).

10. Reference 5, Section 3.3.
We have used σ (pomeron) = 15.18 mb $P_{lab}^{0.0755}$ = 22.13 mb at 147 GeV/c.

11. D. Fong et al., Average Charged Multiplicities in Inclusive Reactions, Phys. Rev. D19 (1979) 743.

12. Average π^o multiplicity is taken to be 0.5 x average γ multiplicity.

13. F. T. Dao and J. Whitmore, Phys. Letters 46B (1973) 252.

14. D. Cohen, Phys. Letters B47 (1973) 457.

15. Z. Koba, H. B. Nielsen and P. Olesen, Nucl. Phys. B40 (1972) 317.

16. Figure 77 in J. Whitmore, Physics Reports 10C (1974) 273.

17. For example, G. H. Thomas, Phys. Rev. D8 (1973) 3042 and R. Kirschner, Nuclear Phys. B101 (1975) 507.

18. Structure has been noted earlier by N. Yamdagni, CERN/D.Ph II/PHYS 75-40.

19. Two particle inclusive cross-sections are for the process $\pi^- p \to a+b+X$ where X can contain a or b. When there are two or more identical particles of interest in the final state, the counting is done such that the inclusive cross-section is the integral of the two-particle density function, e.g., a final state 2γ contributes twice to $\sigma(\gamma\gamma)$, a state 3γ contributes six times to $\sigma(\gamma\gamma)$. Thus $\sigma(aa) = \langle n_a(n_a-1)\rangle\sigma_{inel}$. The pair counts given in Table II, conversely, count pairs of particles without regard to permutation, e.g., final state 3γ contributes a count of 3 to the $\gamma\gamma$ pair count.

TABLE I Neutral Vertex Counts

	27K Sample	70K Sample	Total
First scan (2 passes)	733	1986	2719
Second independent scan	196	-	196
Total	929		2915

Total sample after cuts for decay volume, minimum length, π^- beam, etc.	2327
Neutral vertices with fits	1896

Ambiguity Resolution:

	After Ionization Check	After p_t Cut	Final Cuts
K_s^o	431	476	505
Λ	175	191	238
$\bar{\Lambda}$	17	31	32
γ	1003	1121	1121
Total Resolved	1626	1819	1896
Ambiguous	270	77	0

Table II Inclusive Cross-sections

	σ(mb)		Particle Count
K_s^o	3.67 ± 0.38		505
Λ	1.65 ± 0.21		238
$\bar{\Lambda}$	0.38 ± 0.13		32
γ	129 ± 10.6		1121
		Total	1896

	σ(mb)[a]	Pair Count[a]
$K_s^o K_s^o$	1.51 ± 0.45	28
$K_s^o \Lambda$	0.60 ± 0.17	31
$K_s^o \gamma$	29.7 ± 6.6	71
$\Lambda\gamma$	12.2 ± 5.7	34
$\gamma\gamma$	1000 ± 200	83

a. See Ref. 19 for definitions of two-particle inclusive cross-sections and pair counts.

FERMILAB-PUB-80-112-E

Table III Central Region Cross-sections

	$d\sigma/dy$ at $y=0$ mb/unit of y	$1/\sigma_{pomeron} \times 1/\pi\ d\sigma/dy$
K°_{s}	1.24 ± 0.19	0.0178 ± 0.0027
positive particles	17.5 ± 1	0.252 ± 0.015
negative particles	16.0 ± 1	0.230 ± 0.015
total charged	33.5 ± 1.4	0.482 ± 0.021
Λ	0.31 ± .11	0.0045 ± 0.0015
$\bar{\Lambda}$	0.20 ± .10	0.0029 ± 0.0015

FERMILAB-PUB-80-112-E

Table IV Comparison of Properties of Central Region Production and Cross-section Increase

	Charged Particles	K_s^o	K_s^o Charged Ratio
Particle density per unit of rapidity $\frac{1}{\sigma_{inelastic}} \times \frac{d\sigma}{dy}\Big\vert_{y=0}$	1.60 ± 0.07	0.059 ± 0.01	(3.7 ± 0.6)%
Multiplicity increase per unit of rapidity $\Delta n/\Delta \ln s$	1.45 ± 0.03	0.045 ± 0.003	(3.1 ± 0.2)%

FERMILAB-PUB-80-112-E

Figure Captions

Fig. 1 Physics bias of scan and measure losses - c.m. rapidity distributions of second pass of scan and of measuring (shaded) compared to overall distribution. Events have been weighted as described in the text.

Fig. 2 χ^2 confidence level distributions for accepted 3C fits.

Fig. 3 Decay angle distributions for K_s^o, Λ, $\bar{\Lambda}$. (a) cos θ polar angle, (b) ϕ azimuthal angle. Fitted quantities have been used and distributions are weighted. Angles are calculated for the negative track in the rest frame of the neutral particle with $\hat{z}$ along the direction of the neutral and $\hat{x}$ perpendicular to the camera axis.

Fig. 4 Weighted distributions of momentum component of negative track from decay, transverse to line of flight of neutral. The solid line is the expected shape for K_s^o.

Fig. 5 Energy dependence of multiplicity of π^o, Λ and $\bar{\Lambda}$ particles in π^-p, pp and π^+p collisions. The straight line in the π^o plot is from Whitmore (reference 5).

Fig. 6 Energy dependence of multiplicity of K_s particles in π^-p pp and π^+p collisions. A fit to all the data of the form $\langle n_k \rangle = A+B \ln s$ is shown. Fits of more complicated form to charged particle multiplicities are shown for comparison, normalized as explained in the text. $K^{\pm}$ production fits are also shown for comparison. These comparison fits are from Antinucci et al. (reference 8) and Stix and Ferbel (reference 7).

Fig. 7 Inclusive distributions (weighted) for K_s^o, Λ, $\bar{\Lambda}$ and γ production in $\pi^- p$ collisions at 147 GeV/c. The distributions are shown as invariant cross-section $d\sigma/dy$ vs. c.m. rapidity y; errors are statistical only. The "plateau" line in the K_s^o plot shows the height of the rapidity plateau predicted (see text) from the slope of the fit to the previous figure.

Fig. 8 Inclusive distributions for K_s^o, Λ, $\bar{\Lambda}$ and γ production in $\pi^- p$ collisions at 147 GeV/c. The distributions are shown as cross-section $d\sigma/dx$ vs. Feynman x; errors are statistical only.

Fig. 9 Inclusive distributions for K_s^o, Λ, $\bar{\Lambda}$ and γ production in $\pi^- p$ collisions at 147 GeV/c. The distributions are shown as invariant cross-section $(2E/\sqrt{s}\ \pi)\ d\sigma/\ dx$ vs. Feynman x; errors are statistical.

Fig. 10 Inclusive distributions for K_s, Λ, $\bar{\Lambda}$ and γ production in $\pi^- p$ collisions at 147 GeV/c. The distributions are shown as cross-section $d\sigma/dp_T^2$ vs. transverse momentum squared p_T^2. The complete range of p_T^2 is shown.

Fig. 11 Same transverse momentum squared distribution as previous figure but for narrow range of p_T^2.

Fig. 12 Variation of average transverse momentum squared as a function of Feynman x for γ, K_s, Λ and $\bar{\Lambda}$ particles in $\pi^- p$ collisions at 147 GeV/c.

Fig. 13 Variation of average transverse momentum squared as a function of rapidity y for γ, K_s, Λ and $\bar{\Lambda}$ particles in $\pi^- p$ collisions at 147 GeV/c.

Fig. 14 Variation of average transverse momentum squared as a function of Feynman x for charged particle production π^-, π^+ and p in $\pi^- p$ collisions at 147 GeV/c. Note that protons are detected only up to 1.4 GeV/c in the laboratory frame.

Fig. 15 Variation of p_T^2 as a function of rapidity y for charged particle production π^-, π^+, and p in $\pi^- p$ collisions at 147 GeV/c. Not that protons are detected only up to 1.4 GeV/c in the laboratory frame.

Fig. 16 Average multiplicity of K_s, Λ, π^o and $\bar{\Lambda}$ particles as a function of associated charged multiplicity. Data from $\pi^- p$ collisions at 100 and 250 GeV/c are shown for comparison.

Fig. 17 Expected energy dependence of graph of average multiplicity of neutral particles vs associated charged multiplicity. The shape of the curve is assumed to be given and the energy dependence is derived in the text.

Fig. 18 Scaling form of plot of average multiplicity of K_s per event as a function of associated charged multiplicity. Abscissa and ordinate are normalized by $\langle n \rangle$ and $\langle K \rangle$ as derived in the text. A compilation of πp and pp data at various energies is shown, and a common hand-drawn curve is shown for reference in comparing K_s and π^o data.

Fig. 19 Scaling form of plot of average multiplicity of π^o per event as a function of associated charged multiplicity. Abscissa and ordinate are normalized by $\langle n \rangle$ and $\langle \pi^o \rangle$ as derived in the text. A compilation of πp and pp data at various energies is shown, and a common hand-drawn curve is shown for reference in comparing K_s and π^o data.

Fig. 20 Scaling form of plot of average multiplicity of Λ per event as a function of associated charged multiplicity. Abscissa and ordinate are normalized by $\langle n \rangle$ and $\langle \Lambda \rangle$ as devised in the text. A compilation of πp and pp data at various energies is shown and the same hand-drawn curve is transferred from the K_s plot for comparison.

Fig. 21 Scaling form of plot of average multiplicity of $\bar{\Lambda}$ per event as a function of associated charged multiplicity. Abscissa and ordinate are normalized by $\langle n \rangle$ and $\langle \bar{\Lambda} \rangle$ as devised in the text. Both πp and pp data are shown and the same hand-drawn curve is transferred from the K_s plot for comparison. Symbols for data points are the same as for Fig. 20.

Fig. 22 Variation of a type of $K_s/\pi^{\pm}$ ratio with charged multiplicity-scaling form of K_s multiplicity per charged track vs. scaling form of charged multiplicity. Symbols for data points are the same as for Fig. 20.

Fig. 23 Variation of a type of $\pi^o/\pi^\pm$ ratio with charged multiplicity-scaling form of π^o multiplicity per charged track vs. scaling form of charged multiplicity. Symbols for data points are the same as for Fig. 20.

Fig. 24 Same scaling plot of average K_s multiplicity vs. charged multiplicity as for Fig. 18 but including only lower energy data for π^-p collisions. The same hand-drawn curve as for previous figures is shown for comparison.

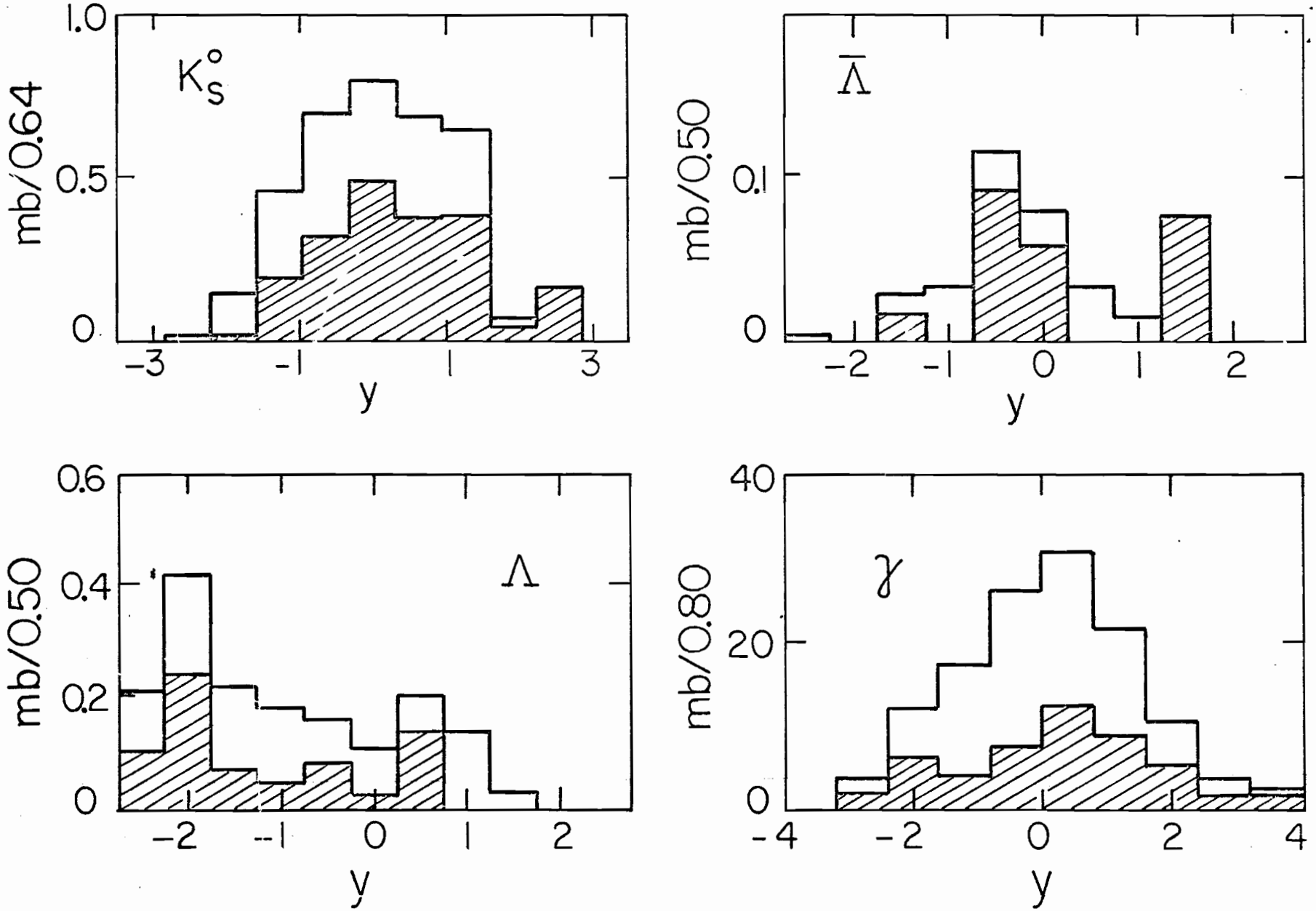
K_S^0
mb/0.64
1.0
0.5
0
-3
-1
1
3
y
$\bar{\Lambda}$
mb/0.50
0.1
0
-2
-1
0
1
2
y
Λ
mb/0.50
0.6
0.4
0.2
0
-2
-1
0
1
2
y
γ
mb/0.80
40
20
0
-4
-2
0
2
4
y

Figure 1

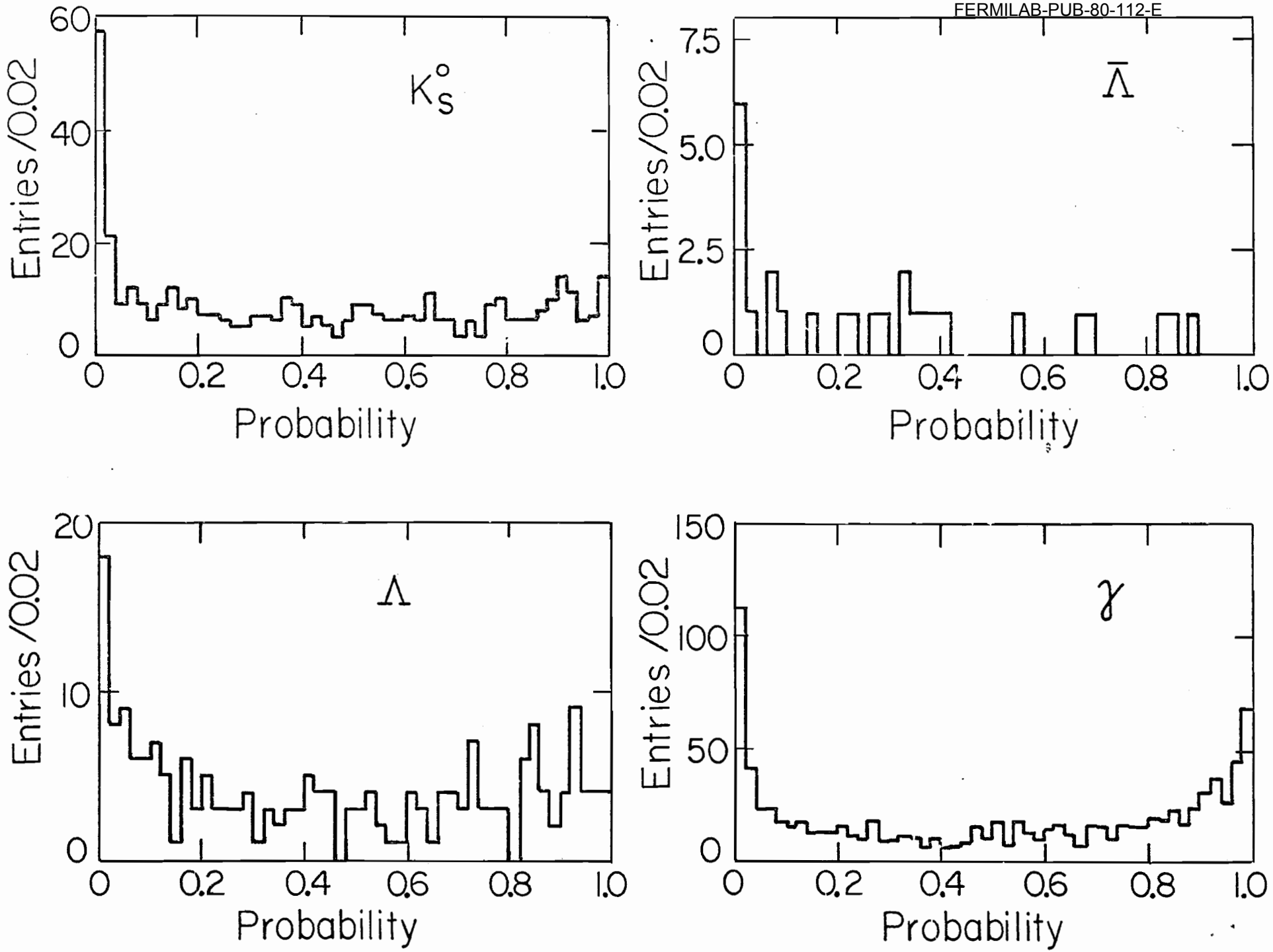
K_S^o
$\bar{\Lambda}$
Λ
γ
Entries/0.02
Probability
0
0.2
0.4
0.6
0.8
1.0
60
40
20
7.5
5.0
2.5
10
150
100
50

Figure 2

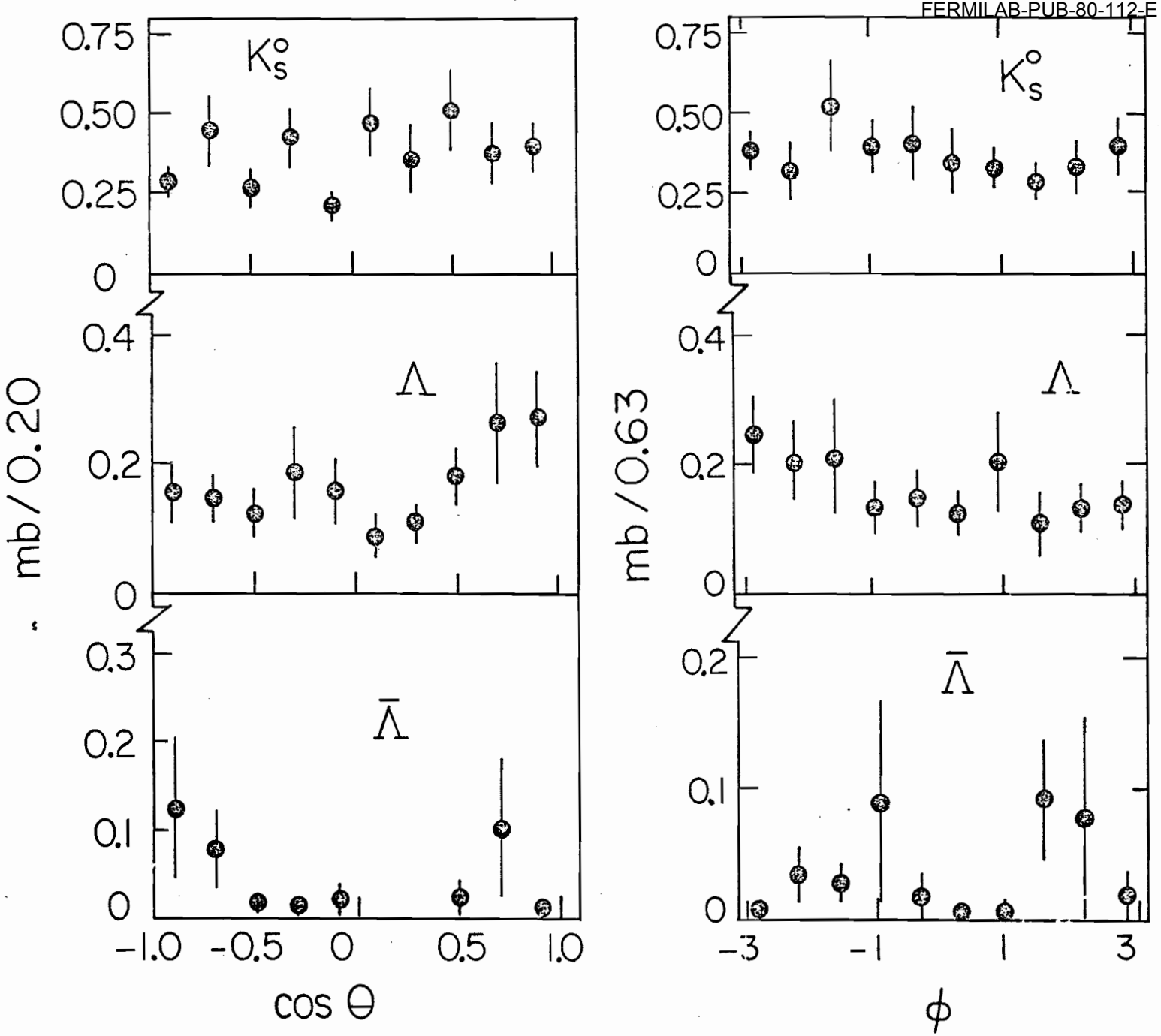

Figure 3

Figure 4 is missing.

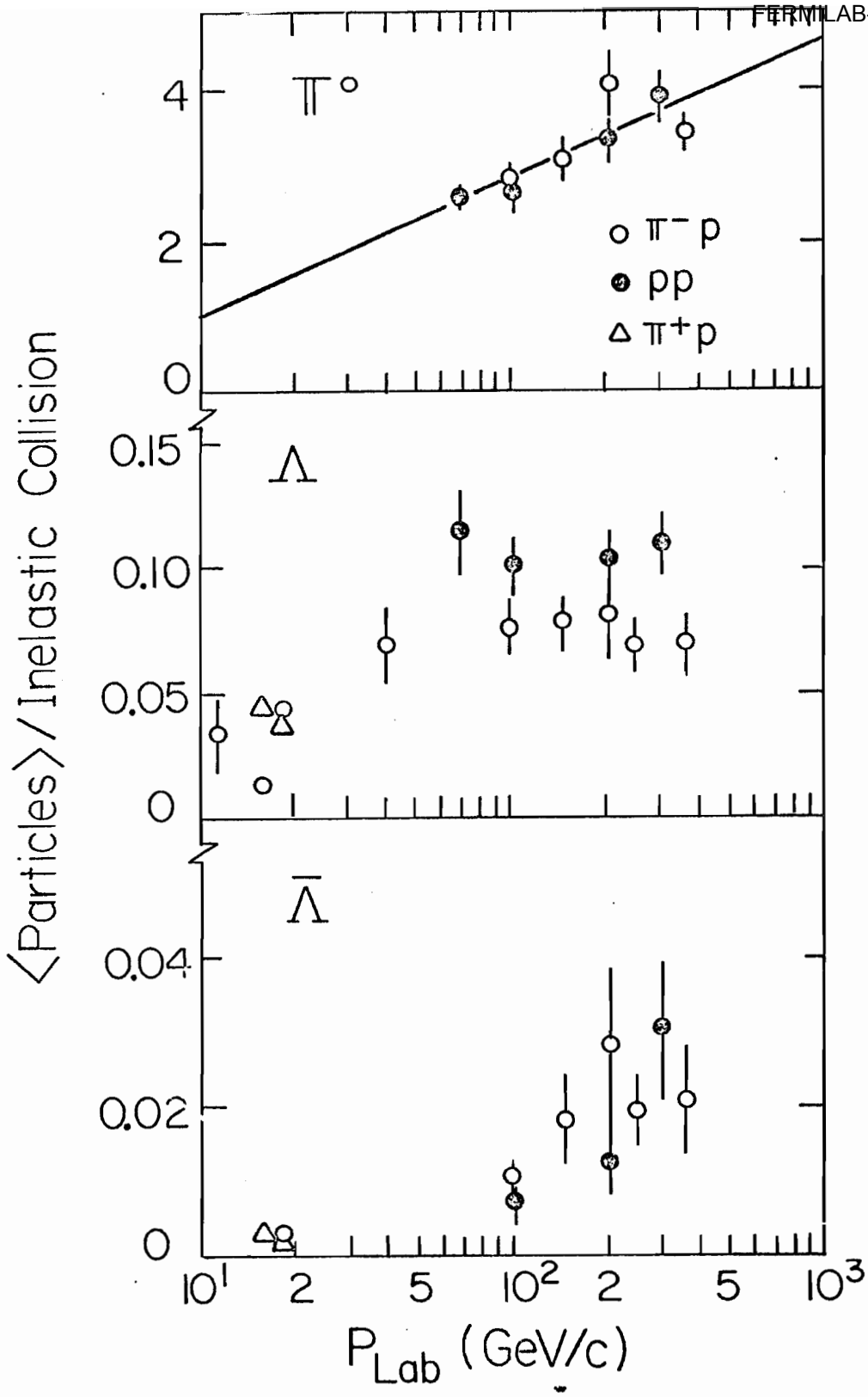
π°
π⁻p
pp
π⁺p
Λ
Λ̄
⟨Particles⟩/Inelastic Collision
P_Lab (GeV/c)
0
2
4
0.15
0.10
0.05
0.04
0.02
10¹
2
5
10²
2
5
10³

Figure 5

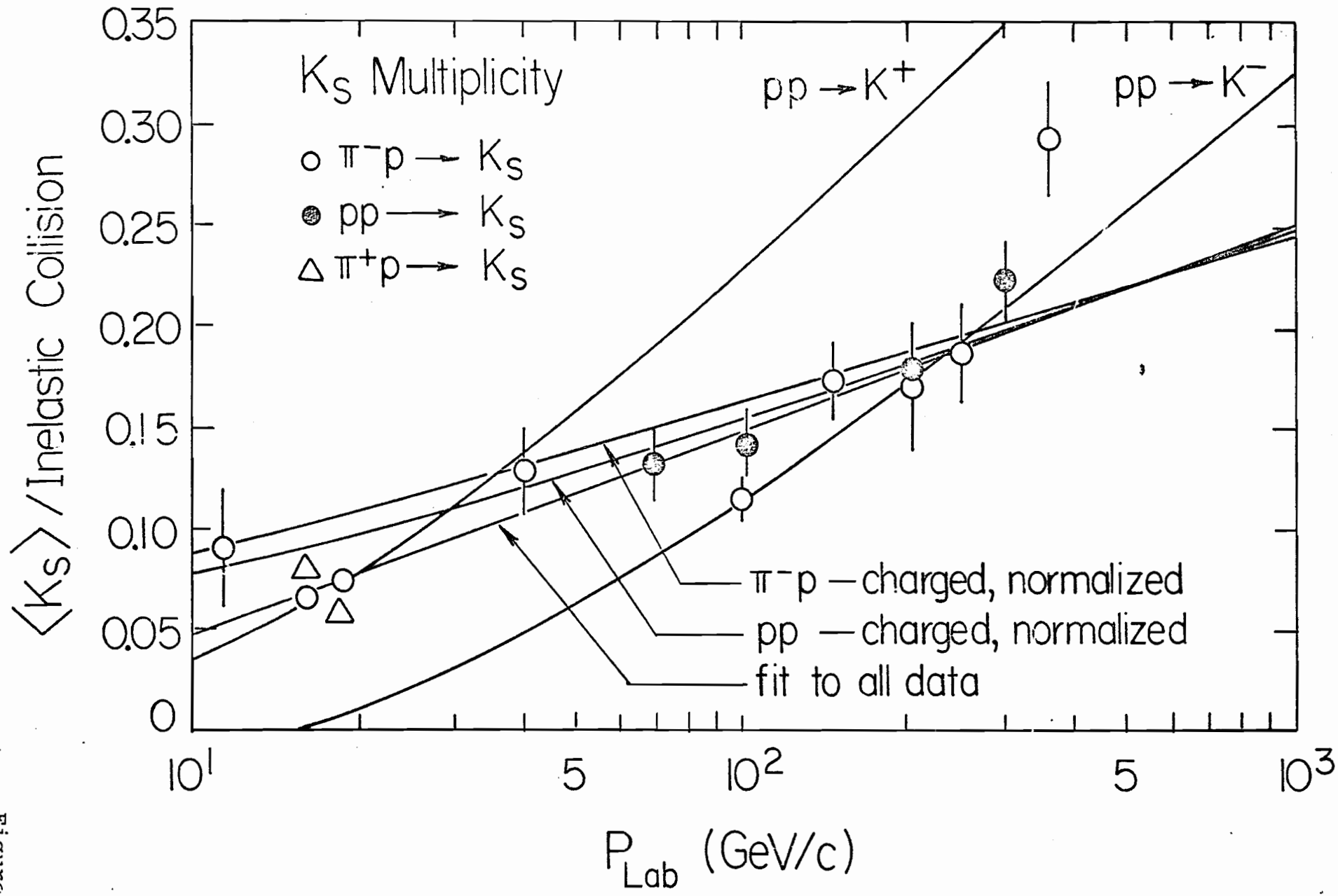
K_S Multiplicity
$\pi^- p \rightarrow K_S$
$pp \rightarrow K_S$
$\pi^+ p \rightarrow K_S$
$pp \rightarrow K^+$
$pp \rightarrow K^-$
$\pi^- p$ — charged, normalized
pp — charged, normalized
fit to all data
$\langle K_S \rangle$ / Inelastic Collision
0.35
0.30
0.25
0.20
0.15
0.10
0.05
0
10^1
5
10^2
5
10^3
P_{Lab} (GeV/c)

Figure 6

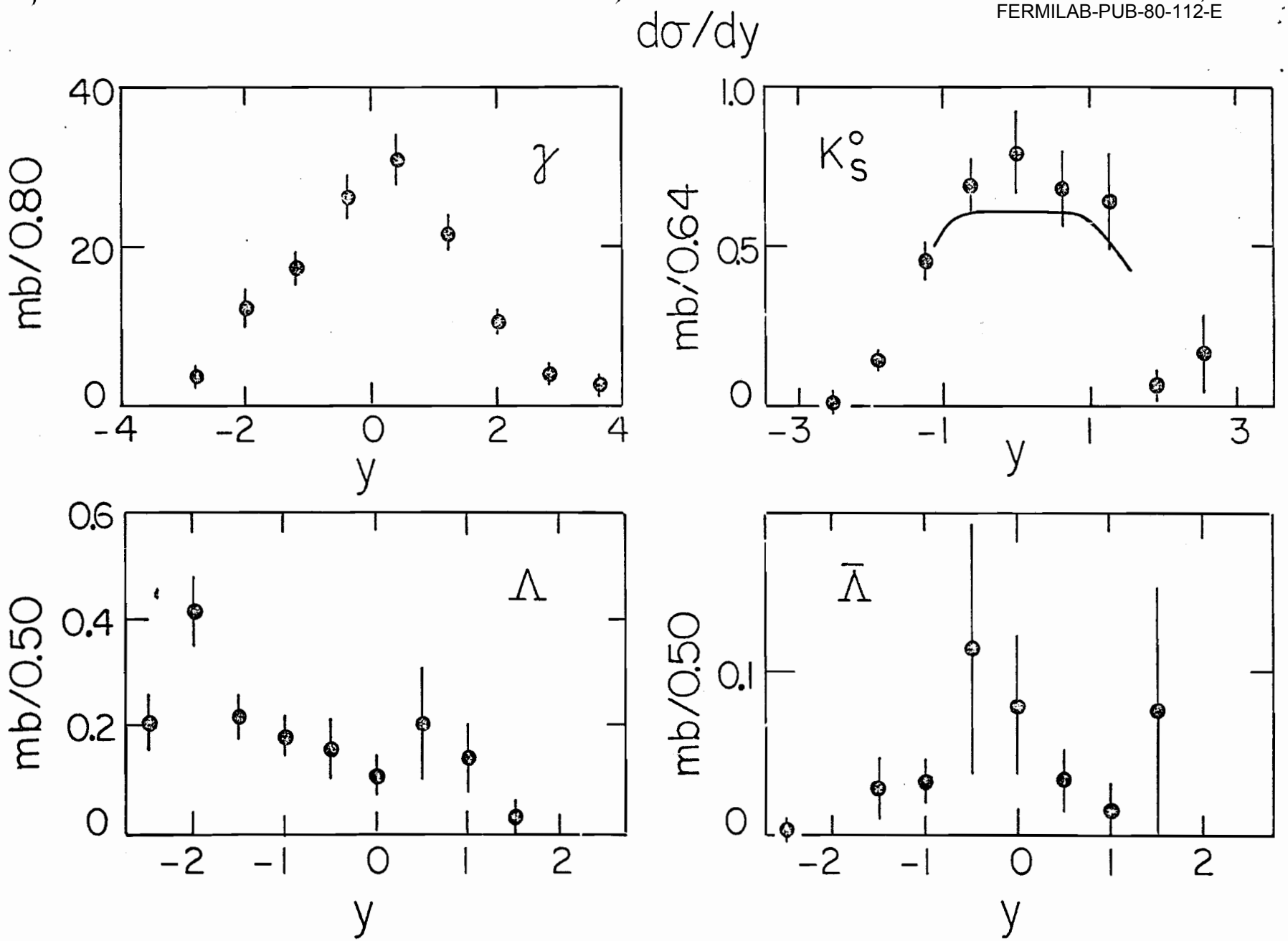

Figure 7

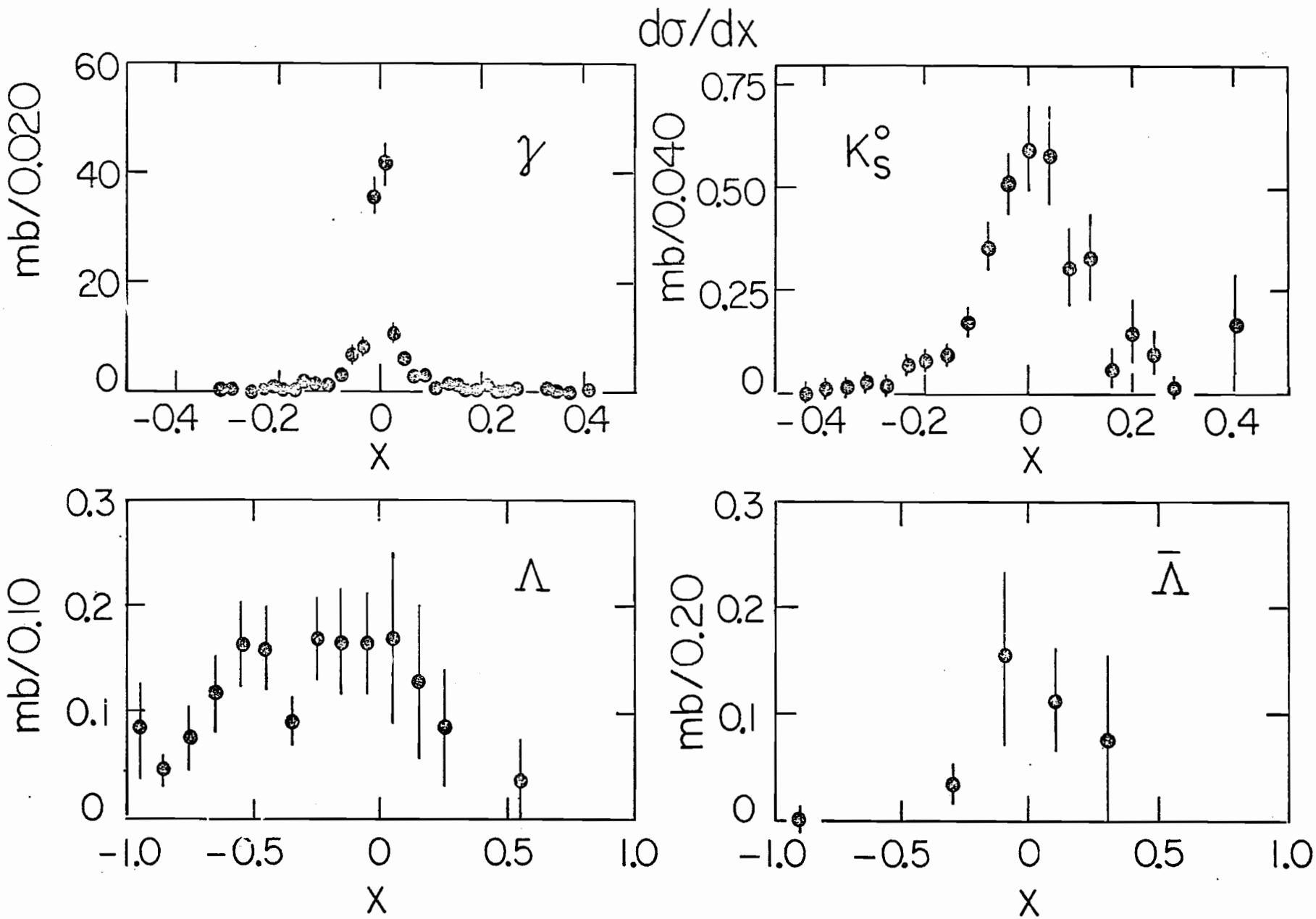
dσ/dx
mb/0.020
60
40
20
0
γ
-0.4
-0.2
0
0.2
0.4
X
mb/0.040
0.75
0.50
0.25
0
K_S^0
-0.4
-0.2
0
0.2
0.4
X
mb/0.10
0.3
0.2
0.1
0
Λ
-1.0
-0.5
0
0.5
1.0
X
mb/0.20
0.3
0.2
0.1
0
$\bar{\Lambda}$
-1.0
-0.5
0
0.5
1.0
X

Figure 8

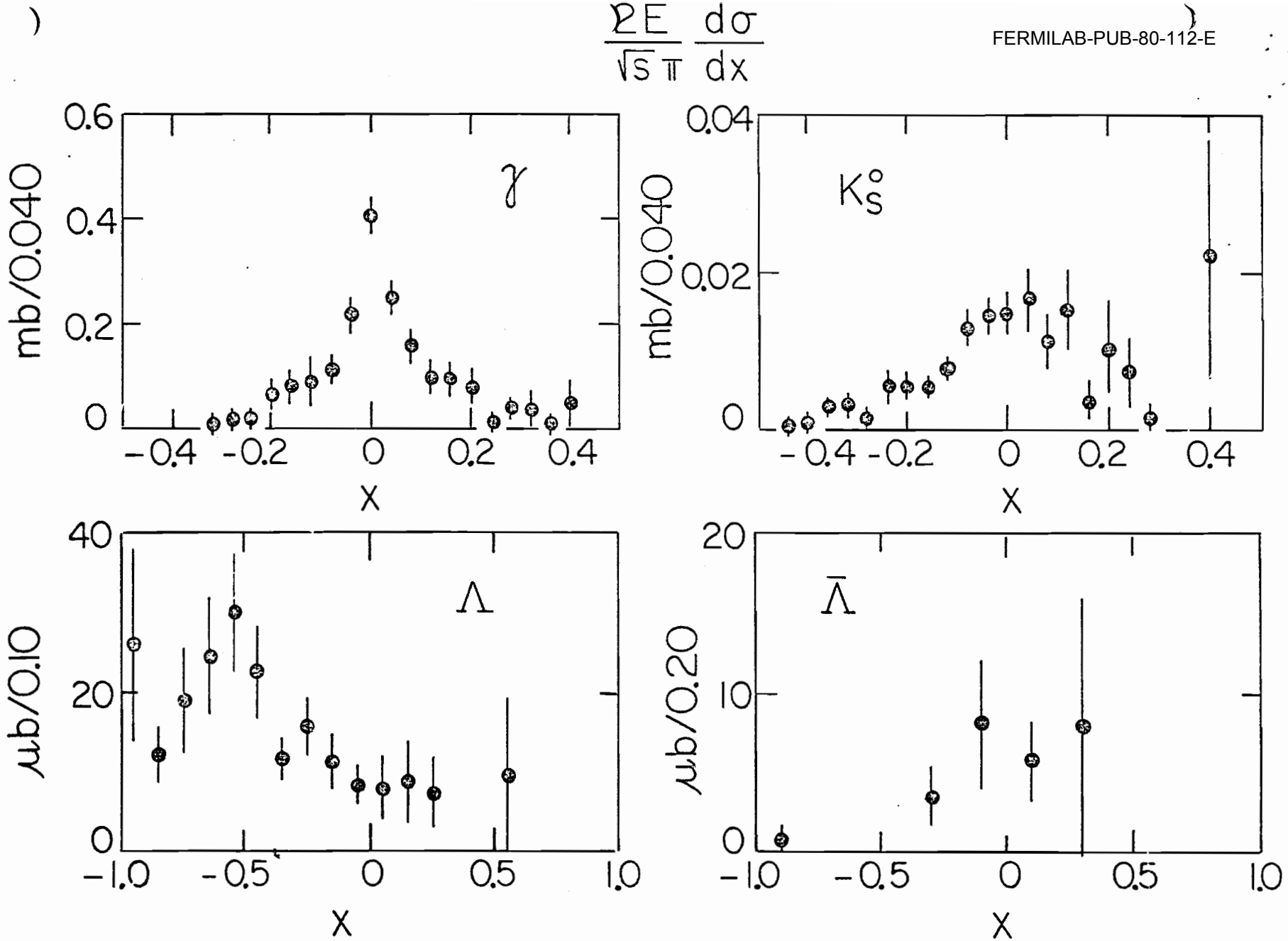
$\frac{2E}{\sqrt{s}\,\pi}\frac{d\sigma}{dx}$
mb/0.040
γ
0.6
0.4
0.2
0
-0.4
-0.2
0
0.2
0.4
X
mb/0.040
K_S^0
0.04
0.02
0
-0.4
-0.2
0
0.2
0.4
X
μb/0.10
Λ
40
20
0
-1.0
-0.5
0
0.5
1.0
X
μb/0.20
$\bar{\Lambda}$
20
10
0
-1.0
-0.5
0
0.5
1.0
X

Figure 9

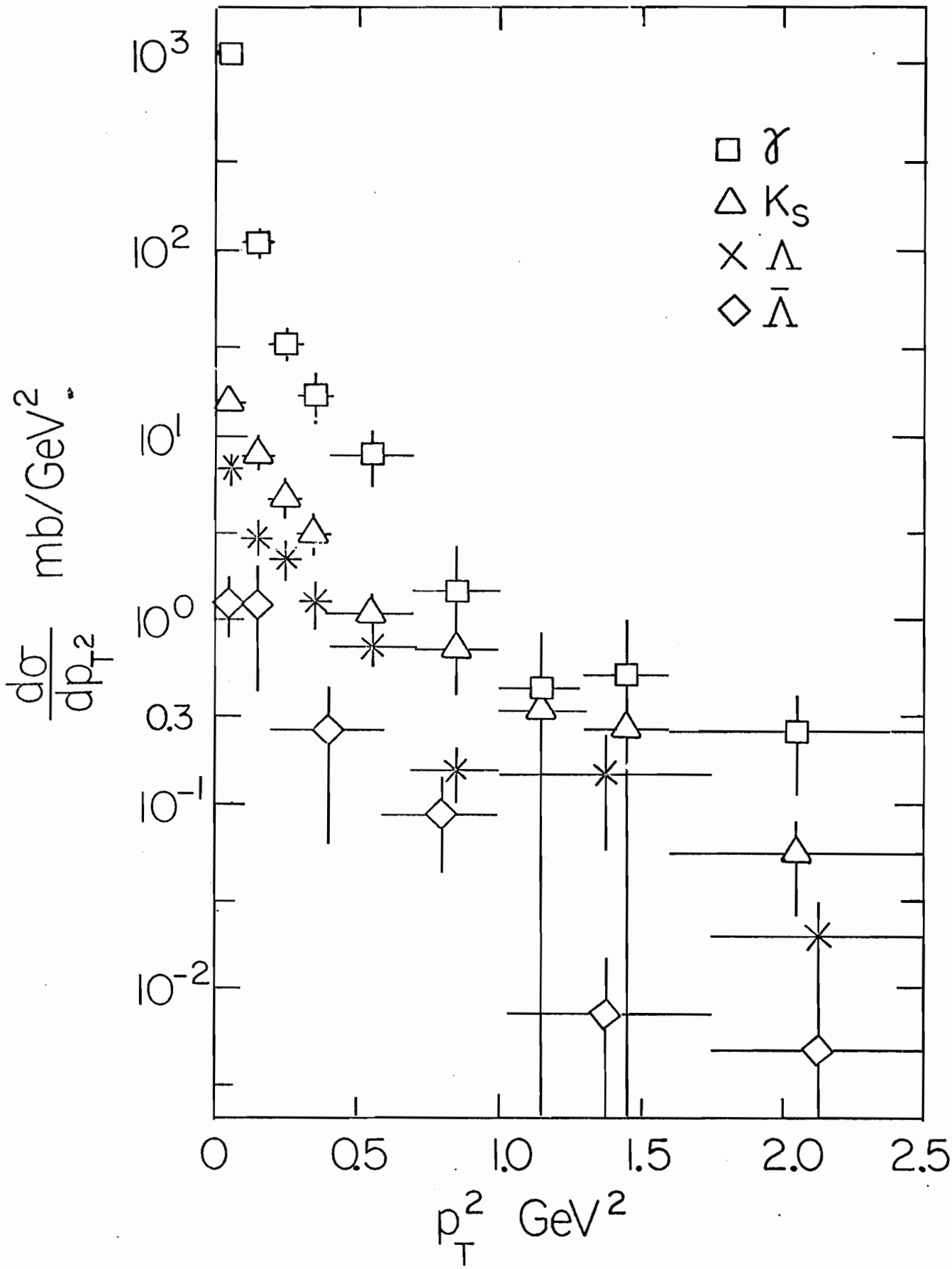
10^3
10^2
10^1
10^0
0.3
10^{-1}
10^{-2}
$\frac{d\sigma}{dp_T^2}$ mb/GeV^2
γ
K_S
Λ
$\bar{\Lambda}$
0
0.5
1.0
1.5
2.0
2.5
p_T^2 GeV^2

Figure 10

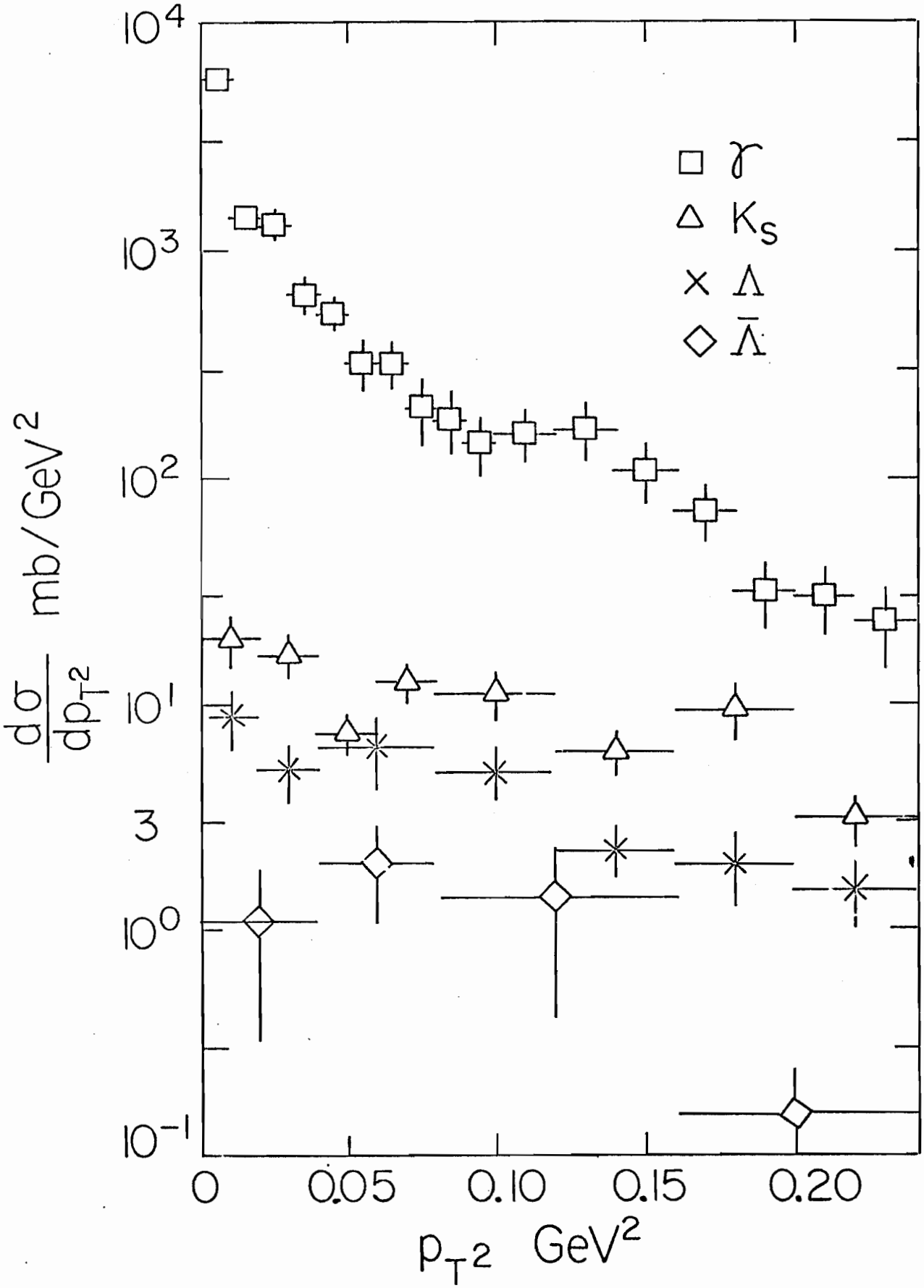
10^4
10^3
10^2
10^1
3
10^0
10^{-1}
$\frac{d\sigma}{dp_T^2}$ mb/GeV^2
γ
K_S
Λ
$\bar{\Lambda}$
0
0.05
0.10
0.15
0.20
p_{T^2} GeV^2

Figure 11

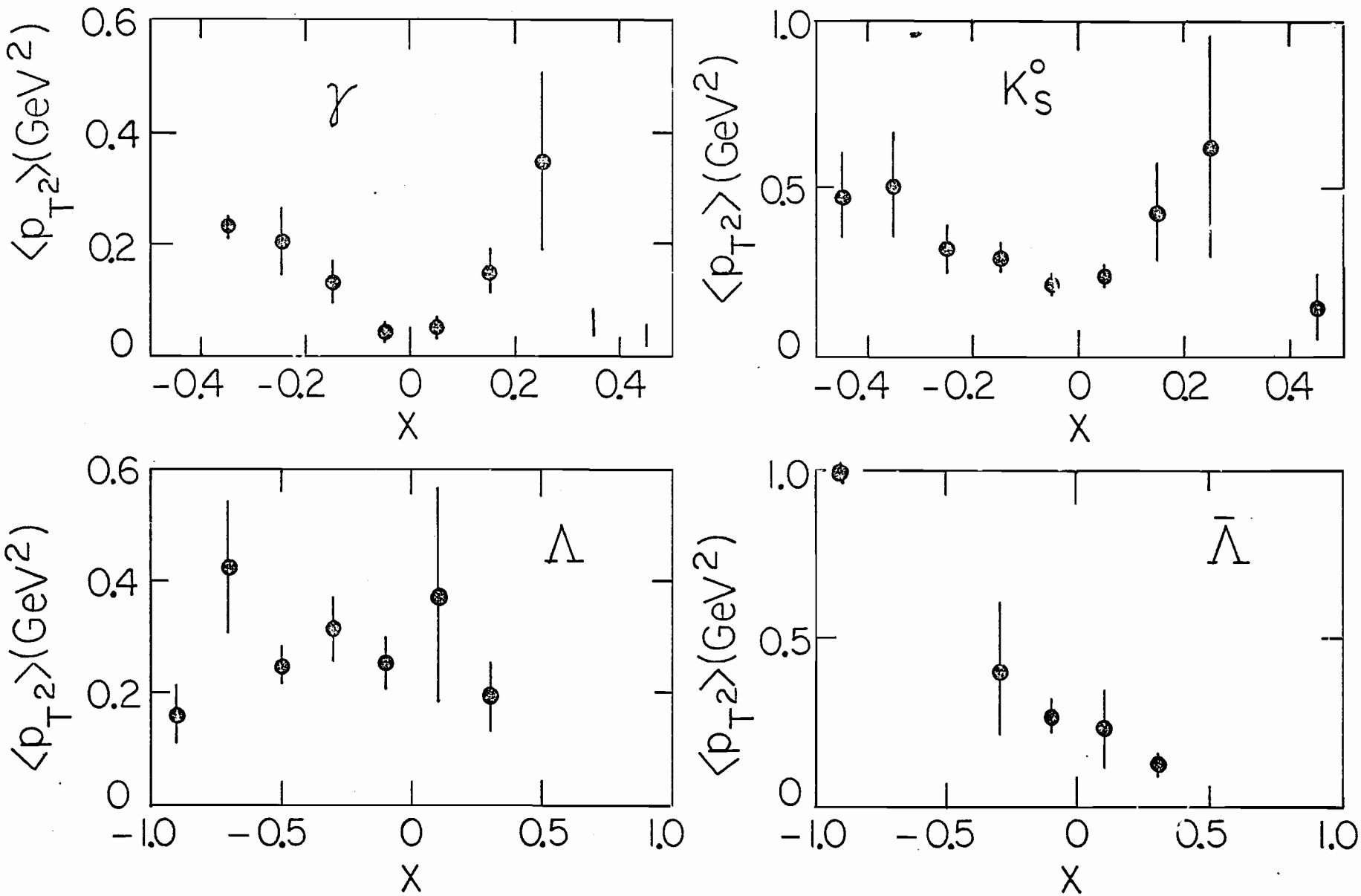
γ
K_S^0
Λ
$\bar{\Lambda}$
$\langle p_{T^2} \rangle$ (GeV^2)
X
0.6
0.4
0.2
0
1.0
0.5
-0.4
-0.2
0.2
0.4
-1.0
-0.5
0.5
1.0

Figure 12

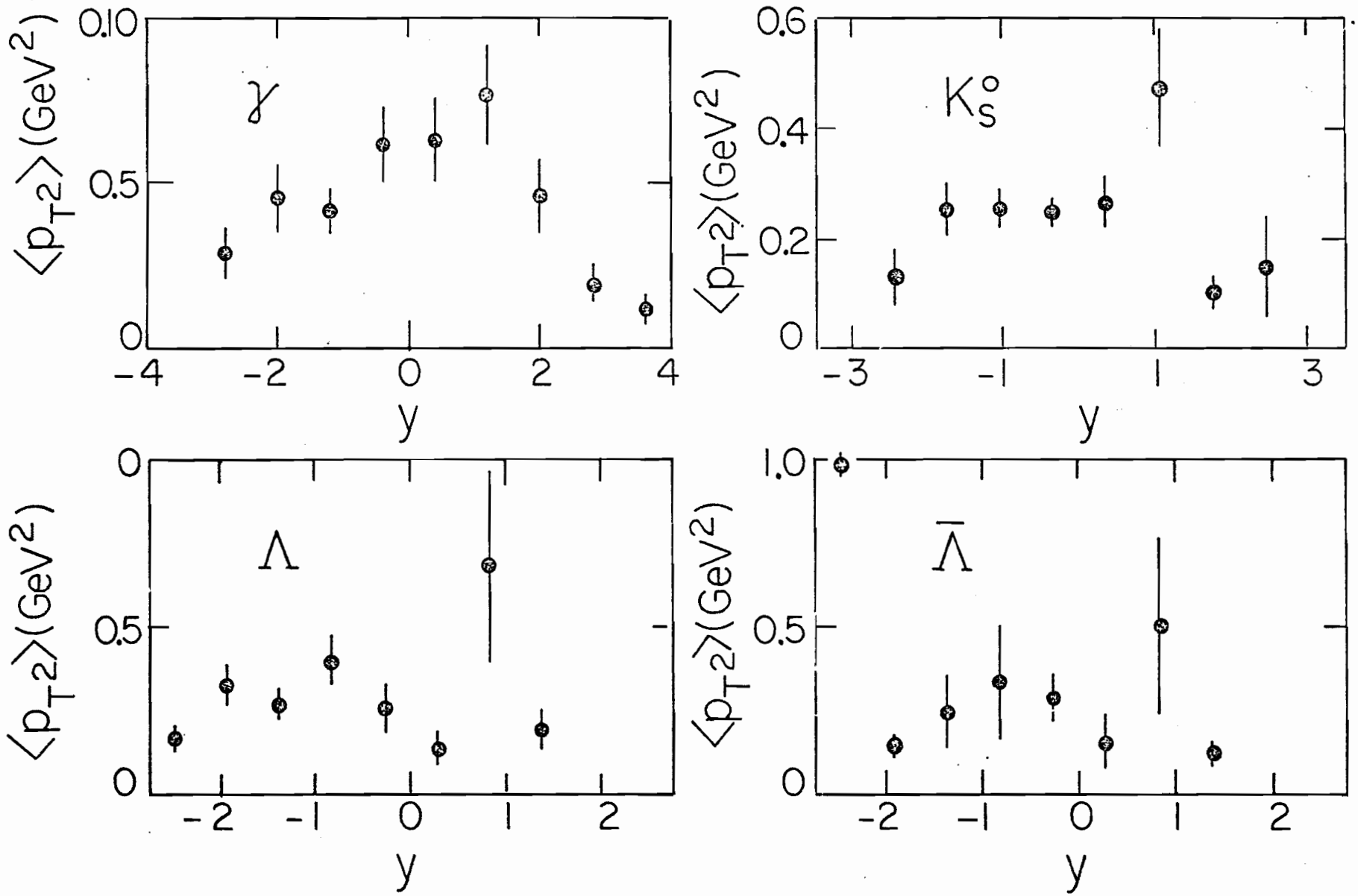
γ
K_S^0
Λ
$\bar{\Lambda}$
$\langle p_{T^2} \rangle (GeV^2)$
y
0.10
0.5
0
0.6
0.4
0.2
1.0
-4
-2
2
4
-3
1
3
-1

Figure 13

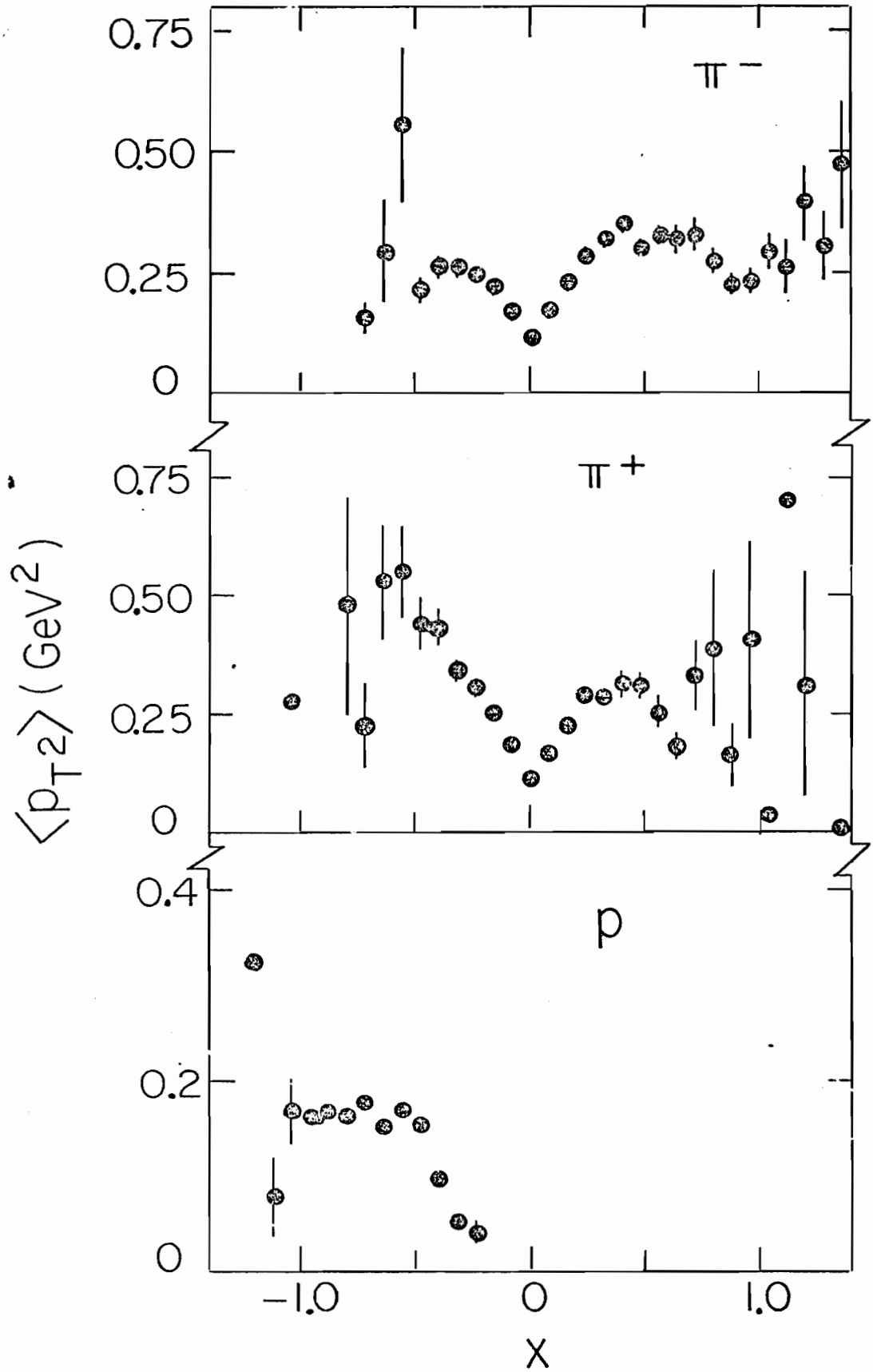

Figure 14

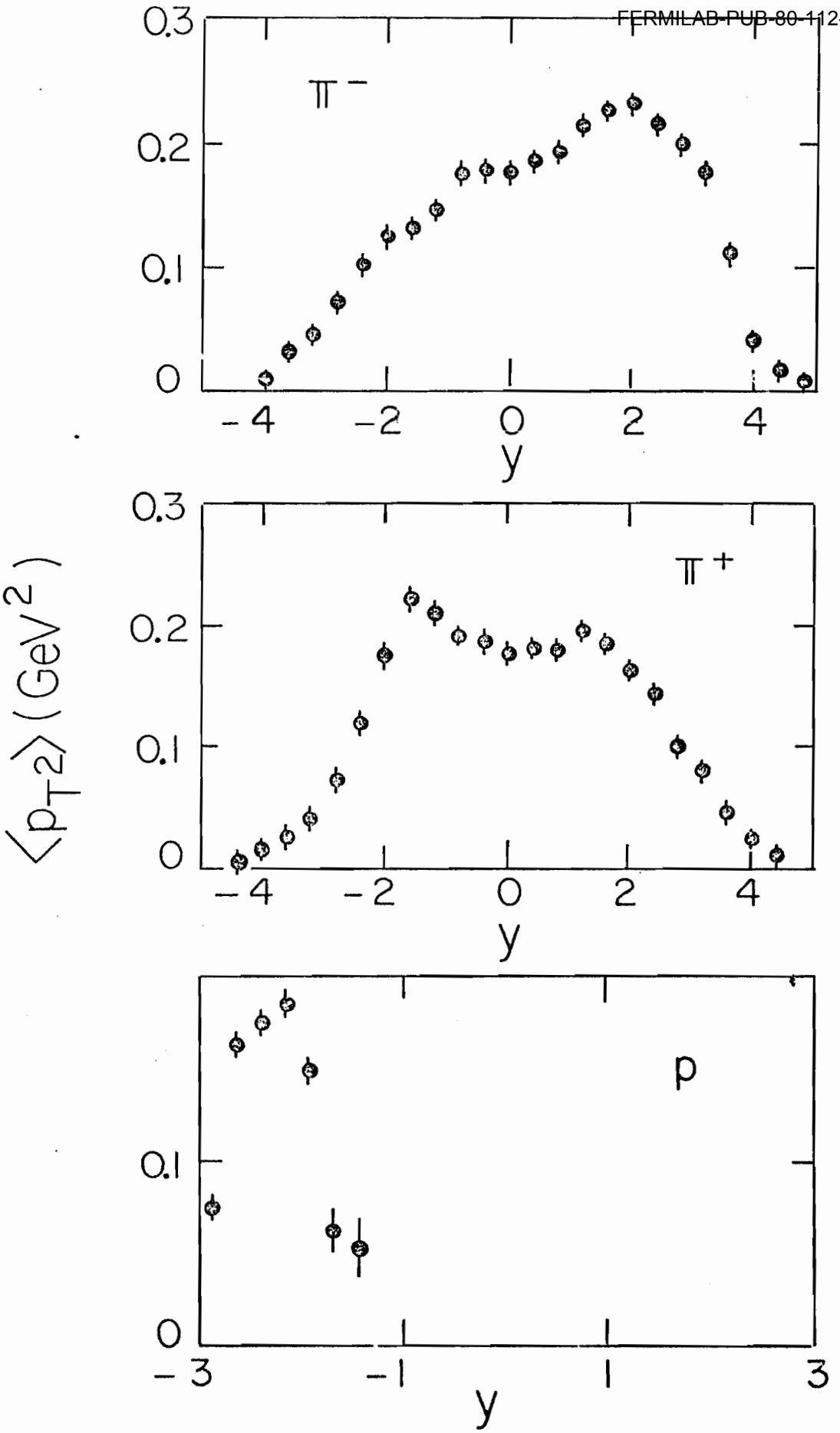
0.3
0.2
0.1
0
π^-
-4
-2
0
2
4
y
0.3
0.2
0.1
0
π^+
-4
-2
0
2
4
y
$\langle p_{T^2} \rangle$ (GeV^2)
0.1
0
p
-3
-1
1
3
y

Figure 15

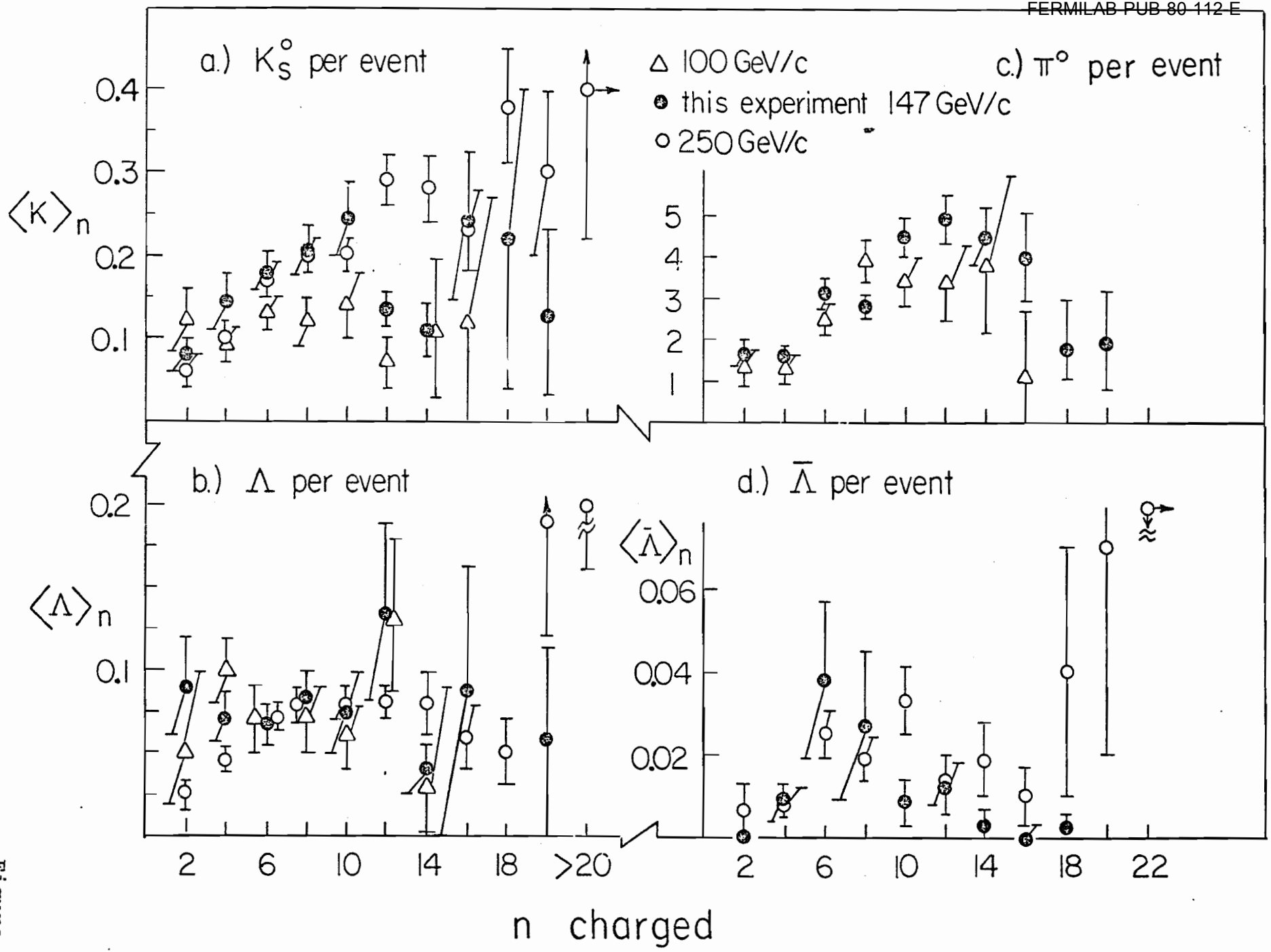
a.) K_S^0 per event
b.) Λ per event
c.) π^0 per event
d.) $\bar{\Lambda}$ per event
△ 100 GeV/c
● this experiment 147 GeV/c
○ 250 GeV/c
$\langle K \rangle_n$
$\langle \Lambda \rangle_n$
$\langle \bar{\Lambda} \rangle_n$
0.4
0.3
0.2
0.1
5
4
3
2
1
0.06
0.04
0.02
2
6
10
14
18
>20
22
n charged

Figure 16

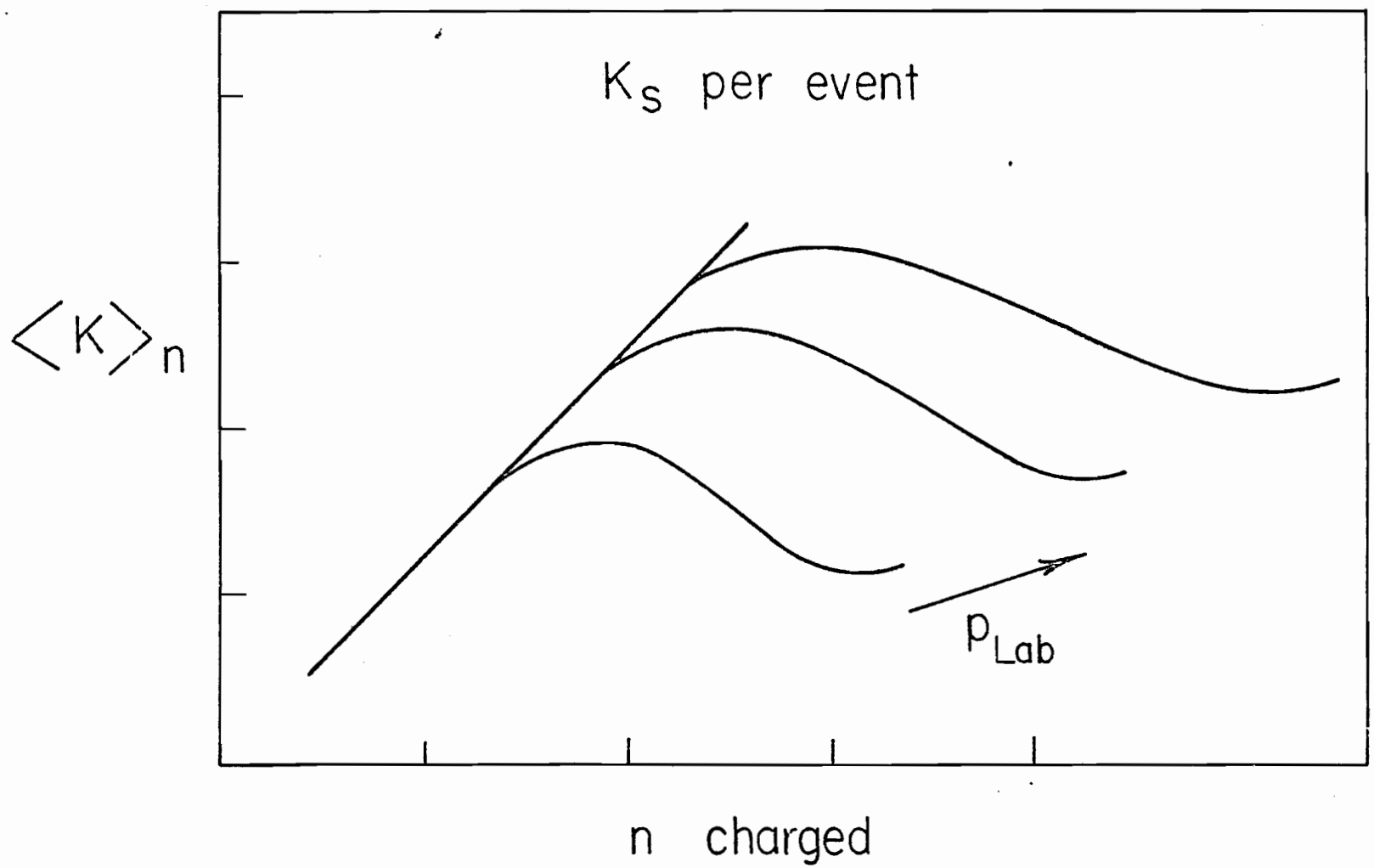

Figure 17

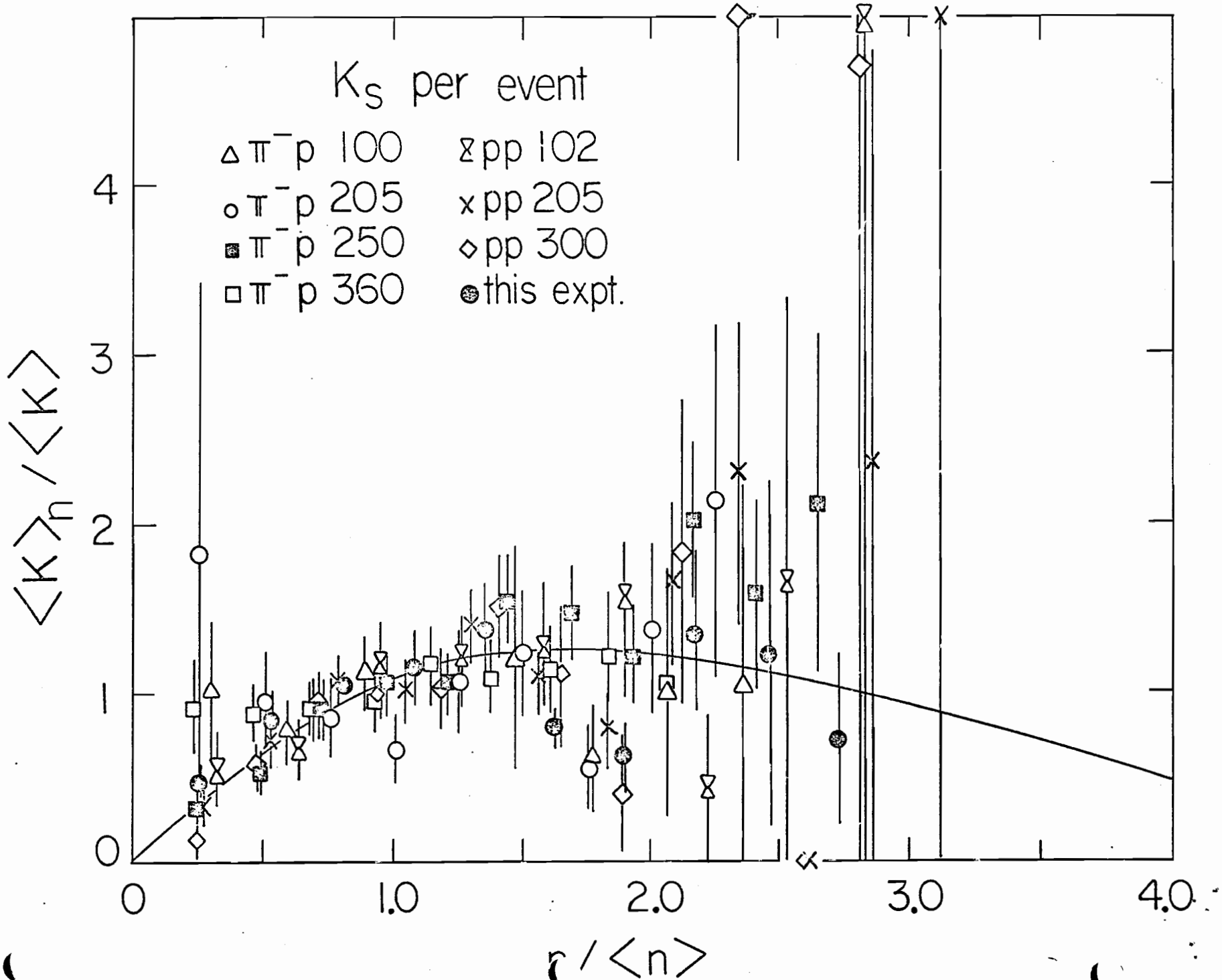
K_S per event
△ π⁻p 100
○ π⁻p 205
■ π⁻p 250
□ π⁻p 360
⧖ pp 102
× pp 205
◇ pp 300
● this expt.
$\langle K \rangle_n / \langle K \rangle$
$r / \langle n \rangle$
0
1
2
3
4
1.0
2.0
3.0
4.0

Figure 18

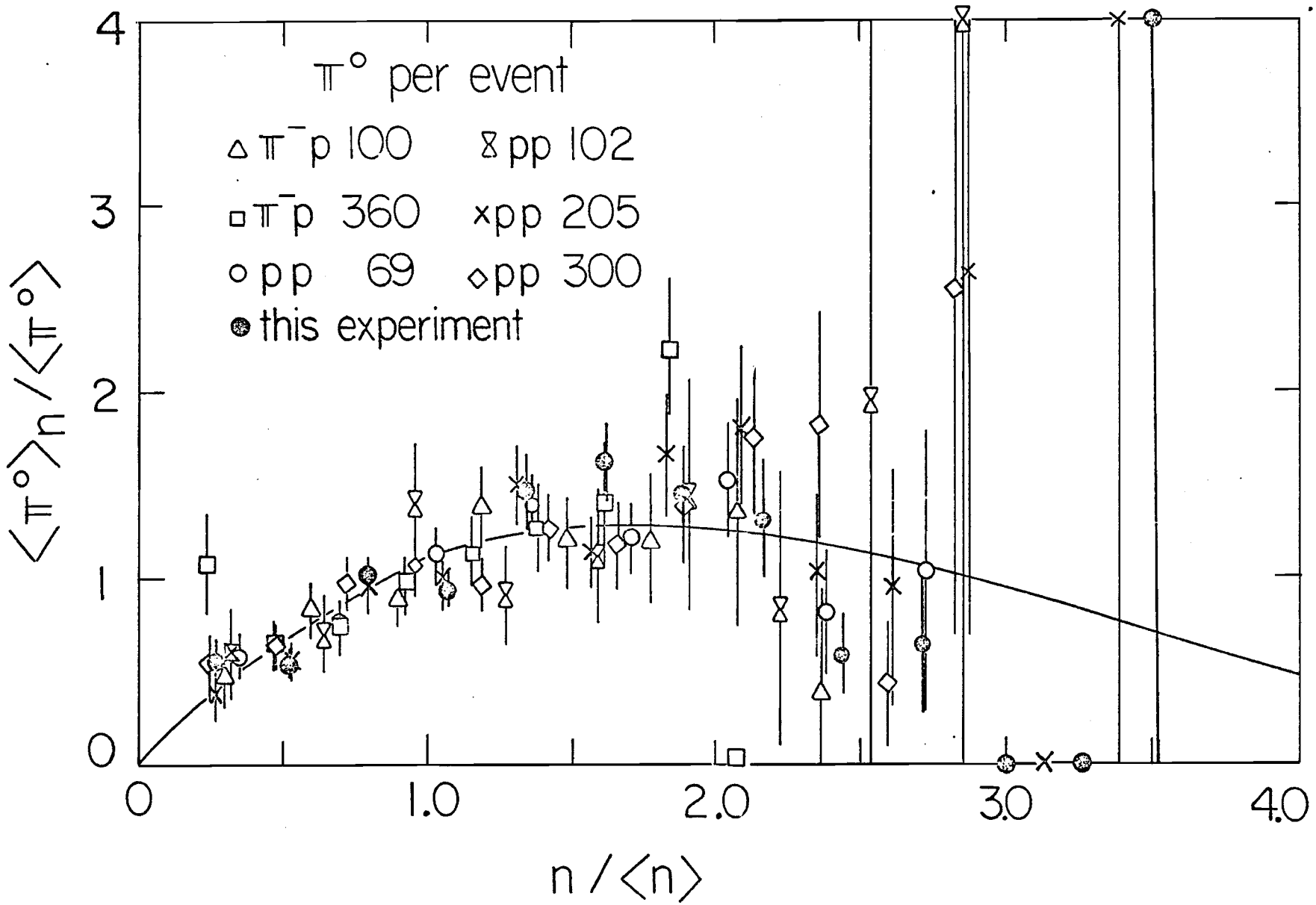
π° per event
△ π⁻p 100
⧖ pp 102
□ π⁻p 360
× pp 205
○ pp 69
◇ pp 300
● this experiment
⟨π°⟩n / ⟨π°⟩
n / ⟨n⟩
0
1
2
3
4
0
1.0
2.0
3.0
4.0

Figure 19

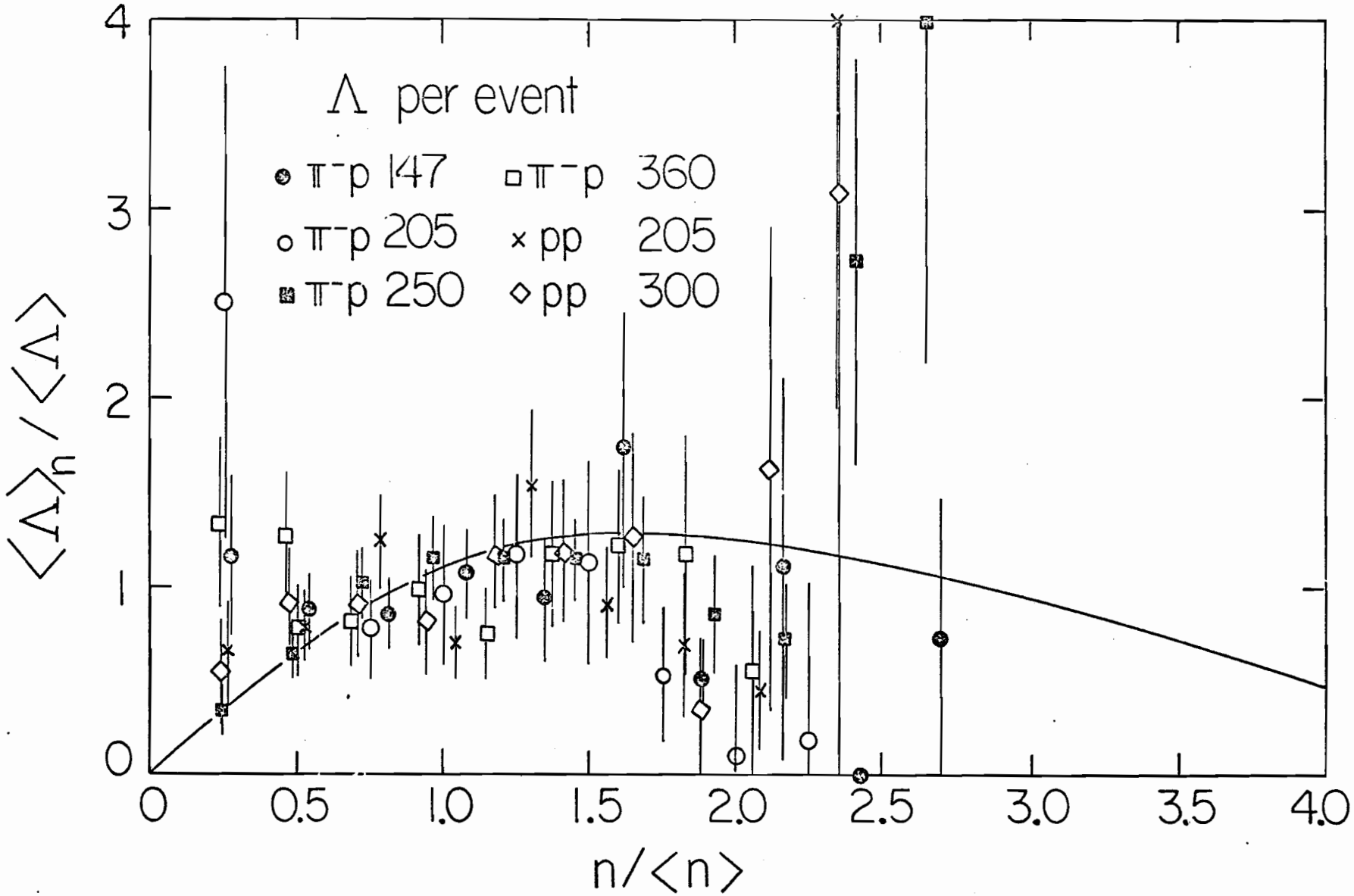
Λ per event
π⁻p 147
π⁻p 360
π⁻p 205
pp 205
π⁻p 250
pp 300
⟨Λ⟩n / ⟨Λ⟩
n/⟨n⟩
0
1
2
3
4
0
0.5
1.0
1.5
2.0
2.5
3.0
3.5
4.0

Figure 20

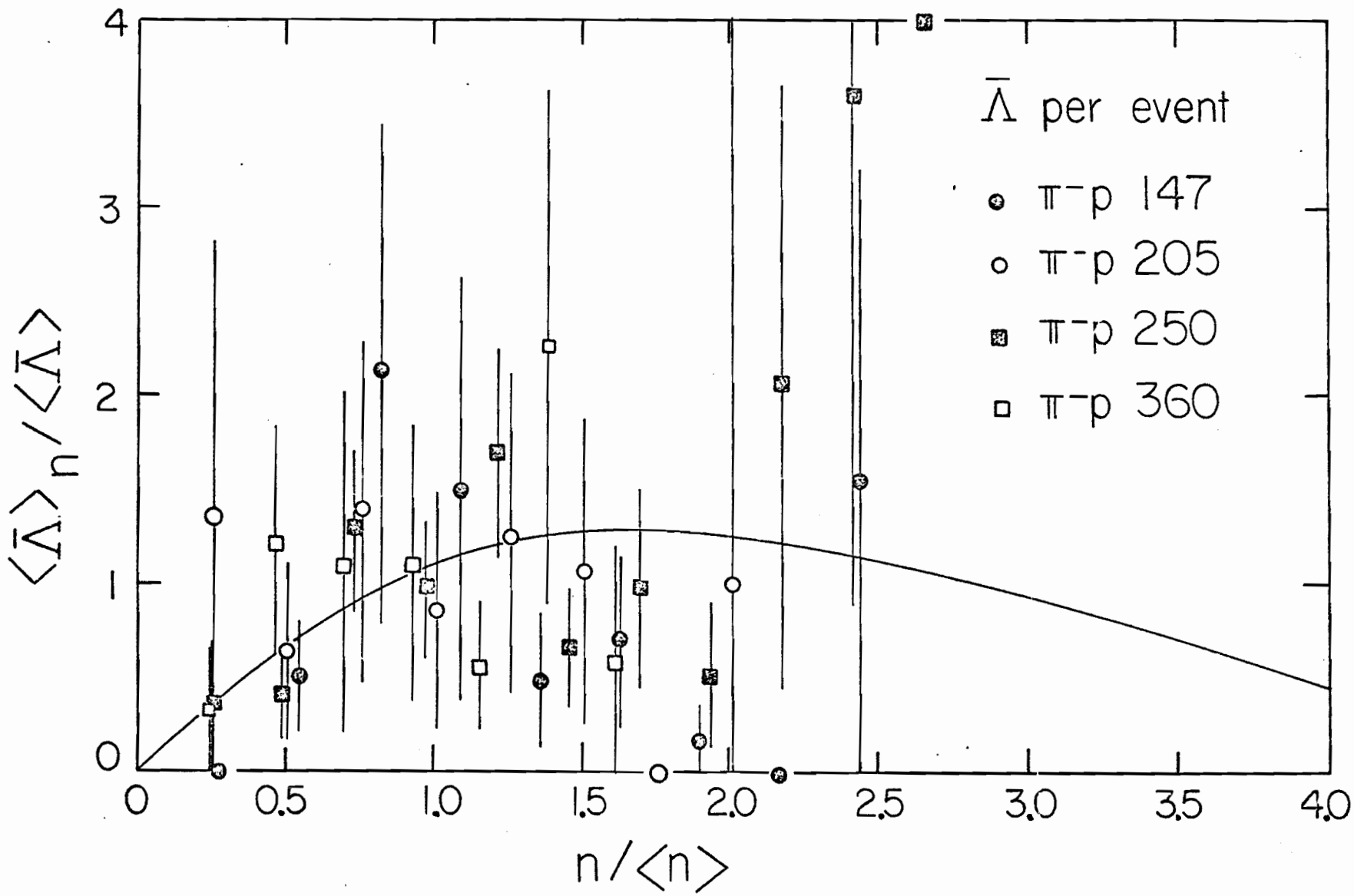
$\bar{\Lambda}$ per event
π⁻p 147
π⁻p 205
π⁻p 250
π⁻p 360
$\langle\bar{\Lambda}\rangle_n/\langle\bar{\Lambda}\rangle$
$n/\langle n\rangle$
0
1
2
3
4
0.5
1.0
1.5
2.0
2.5
3.0
3.5
4.0

Figure 21

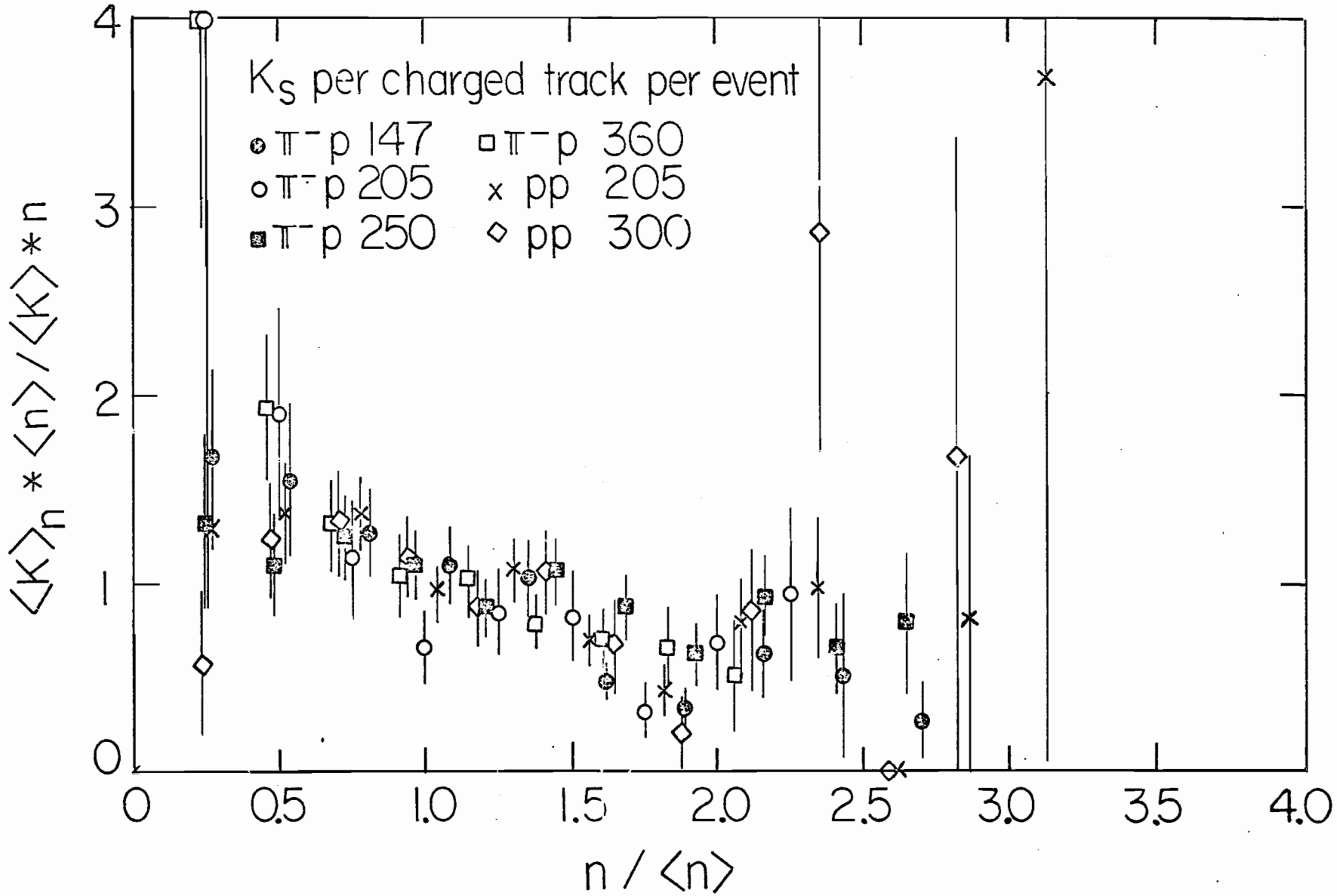
K_S per charged track per event
π⁻p 147
π⁻p 360
π⁻p 205
pp 205
π⁻p 250
pp 300
$\langle K\rangle_n * \langle n\rangle / \langle K\rangle * n$
$n / \langle n\rangle$
0
1
2
3
4
0
0.5
1.0
1.5
2.0
2.5
3.0
3.5
4.0

Figure 22

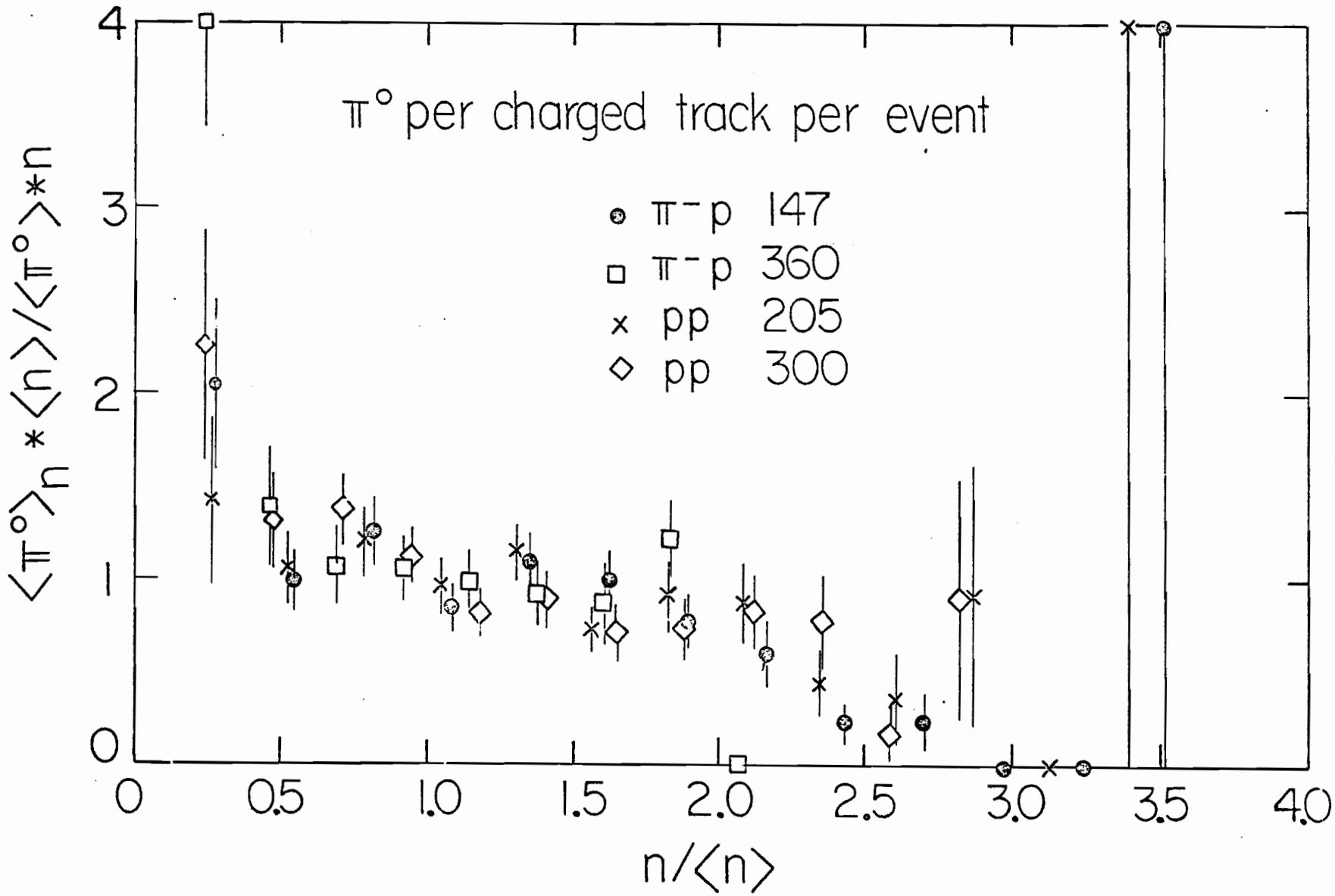
π° per charged track per event
π⁻p 147
π⁻p 360
pp 205
pp 300
⟨π°⟩n * ⟨n⟩/⟨π°⟩*n
n/⟨n⟩
0
1
2
3
4
0
0.5
1.0
1.5
2.0
2.5
3.0
3.5
4.0

Figure 23

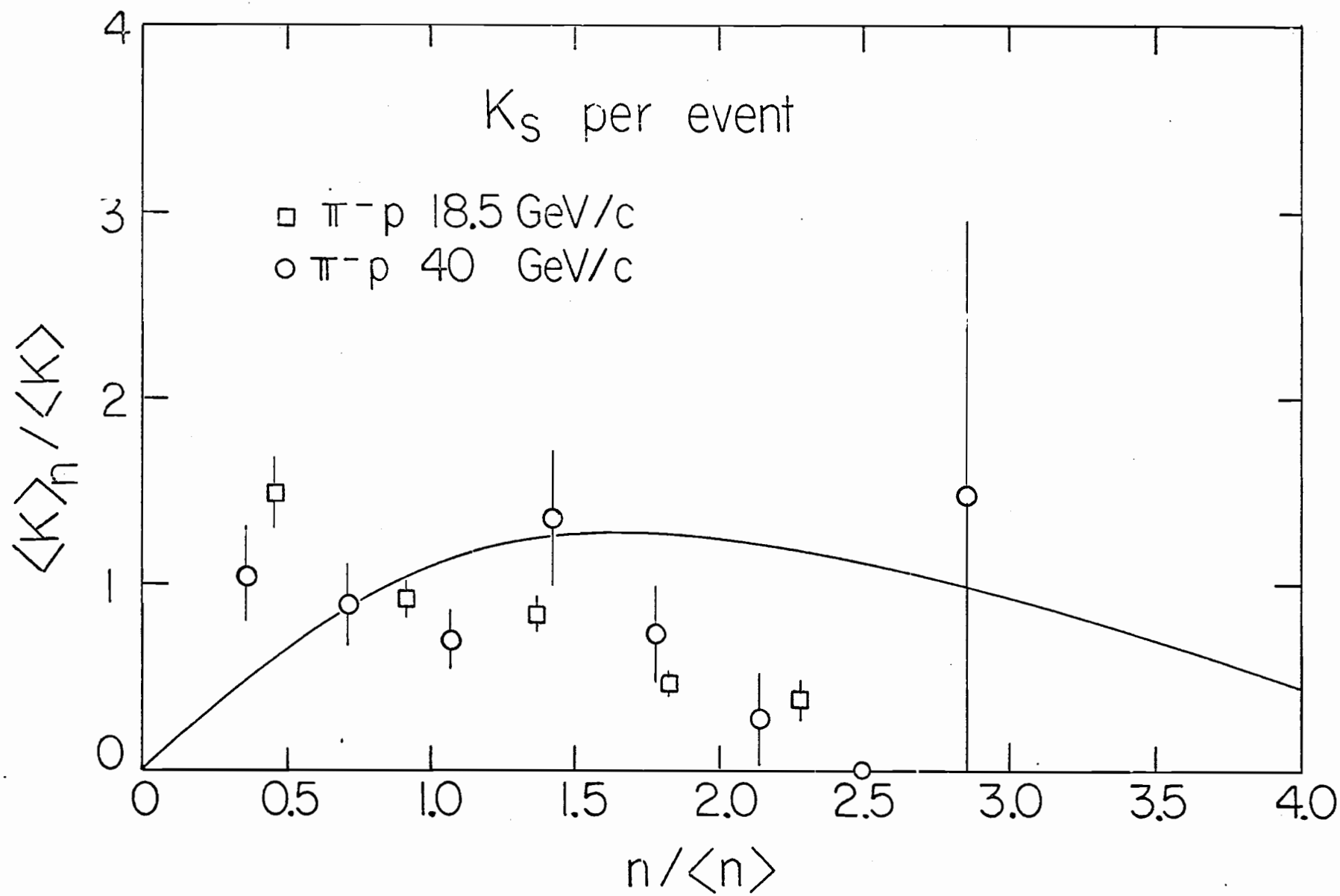
K_S per event
□ $\pi^- p$ 18.5 GeV/c
○ $\pi^- p$ 40 GeV/c
$\langle K \rangle_n / \langle K \rangle$
$n/\langle n \rangle$
0
1
2
3
4
0
0.5
1.0
1.5
2.0
2.5
3.0
3.5
4.0

Figure 24